Synthesis and characterization of Polymer/Graphene electrospun nanofibers

by

Farshad Barzegar

Submitted in partial fulfilment of the requirements for the degree

Master of Science

In the Faculty of Natural & Agricultural Sciences

University of Pretoria

Pretoria

December 19, 2013

Declaration of Originality

I, **Farshad Barzegar** declare that the thesis/dissertation, which I hereby submit for the degree **master** at the University of Pretoria, is my own work and has not previously been submitted by me for a degree at this or any other tertiary institution.

Signature: ……

Date: ……

Dedicated to my parents

This dissertation is dedicated to my beloved parents whose prayers & encouragement have been always with me. I am indebted to them for their support, guidance and encouragement.

Abstract

Polymer nanofibers have attracted a lot of industrial interest in the past decade. In general, these fibers need to be thermally stable for many applications, such as in the aerospace industry. However, most of these polymer nanofibers suffer from low temperature degradation, limiting their use in many potential applications. Graphene, which is one sheet of graphite, has unique properties such as high conductivity, and high thermal stability. This exceptional material can be incorporated into the polymer nanofibers as nanofillers in order to enhance their thermal properties.

The aim of this dissertation is to investigate the effect of adding graphene nanofillers into the polymer fiber on the resulting fibers' thermal properties. For that purpose, polyvinyl alcohol (PVA), a non-conductive polymer and a different source of graphene, namely graphene foam, expendable graphite and graphite powder were used. The growth technique was the electrospinning technique which offers a variety of parameters that need to be optimized. For this includes, the amount of PVA in the water solvent, the flow rate, the applied voltage, the growth time, and the tip/collector distance. In summary, it has been optimized that the best conditions for growth of fibers will be as follows: PVA concentration will be fixed at 10 wt%, flow rate will be 3 ml/h, applied voltage will be 30 kV, growth time of 60 s and tip/collector distance will be fixed at 12 cm. The resulted PVA fibers from these conditions were smooth continuous and hollow with diameter ranging between 190-340 nm, while PVA/graphene nano-fibers are much thinner with diameter ranging between 132 - 235 nm when the same parameters were used with only graphene concentration varied.

The fiber obtained with PVA showed a hollow structure which is desirable for incorporation of graphene nanofillers. The dispersion of the different source of graphene sheets in the starting PVA solution showed enhanced thermal stability compared to the PVA fibers alone. Furthermore, an increase in the thermal stability is observed with increasing concentration of graphene nanofillers.

This work shows the promising use of graphene as nanofillers for PVA fibers. This can be expended to other non-conductive and conductive polymers in order to broaden the application of these fibers in the industries, where thermal stability is a prerequisite.

ACKNOWLEDGEMENTS

I would never have been able to finish my dissertation without the guidance of my Supervisor, Prof. Ncholu Manyala for the faith and support that he has shown me. I would like to express my gratitude towards my colleagues Dr. Julien Dangbegnon, Dr. Saleh Khamlich, Mopeli Fabiane, Abdol Hakim Bello, Damilola Momodu and Fatemeh Taghizadeh who have given me the support and have helped me to finish this work.

I would also like to thank Prof. Chris Theron who believed in me and helped me with my studies and Mrs. Linda Prinsloo and Mrs. Isbe van der Westhuizen for their petitions and help throughout my research.

Finally, I would like to thank my parents, my brothers and my uncle for their love, encouragement and total support in every way possible.

Contents

List of Figure

List of Table

LIST OF ABBREVIATIONS

GO	Graphene-oxide
DP	Degree of polymerization
CMC	Ceramic matrix composites
MMC	Metal matrix composites
PMC	Polymer matrix composites
FRC	Fiber reinforced composite
PRC	Particle reinforced composites
PVAc	polyvinyl acetate
PVA	Polyvinyl alcohol
PPy	Polypyrrole
CNTs	Carbon nanotubes
SWNTs	Single-wall nanotubes
MWNTs	Multi-walled nanotubes
CVD	Chemical vapor deposition

CA	Carbon arc discharge
PLV	Pulsed-laser vaporization
HipCO	High-pressure CO
PMMA	Polymethylmethacrylate
G foam	Graphene foam
EG	Expanded graphite
G powder	graphite powder
SDS	Sodium dodecyl sulfate
TGA	Thermo gravimetric Analysis
SEM	Scanning electron microscope
wt. %	Weight %
ml	Milliliter
g	Gram
KV	kilovolt
S	Second
cm	Centimeter
rpm	Revolutions per minute

˚C	Degree Celsius
mW	Mill watt

LIST OF SYMBOLS

η	Viscosity
η_0	Solvent viscosity
η_{rel}	Relative Viscosity
η_{sp}	Specific viscosity
$[\eta]$	Intrinsic viscosity
K	Constant in Mark–Houwink–Sakurada equation
T_g	Glass Transition Temperature
T_m	Melting point
Q	Rate of flow
ρ	Density
σ	Surface tension
K_e	Electrical conductivity
ε_i	Electrical permittivity

CHAPTER 1

INTRODUCTION

Natural fibers have been used in all cultures for making utilitarian products. Natural fibers can be extracted from the bark (banana, jute, hemp, and ramie), stem (banana, palm, and bamboo), leaf (palm, screw pine, sisal, and agave), husk (coir), seeds (cotton), and grass (sikki, madhurkati, benakati, and munj). Animal fibers are obtained from a variety of animal coats, and insect fibers from cocoons. Rayon was the first factory where man- made fibers were developed. Man-made fibers were made from wood or cotton pulp and were first known as artificial silk. Both natural and man-made fibers have had a significant impact on human beings' everyday lives [1].

In 1897, Thomas Edison used carbon fibers as filaments for preliminary light bulbs. Although these fibers lacked the tensile strength of today's carbon fibers, their considerable tolerance to heat made these fibers ideal for conducting electricity. Those carbon fibers were made out of cellulose-based materials (such as cotton or bamboo), unlike the petroleum-based precursors used today. Such fibers were made from baking bamboo filaments at high temperatures in a controlled atmosphere. This method is known as pyrolysis.

In 1958, Roger Bacon discovered the first high performance carbon fibers. Rayon became the first precursors used to create these modern fibers. These carbon fibers are polymers of

graphite, a pure form of carbon where the atoms are arranged in big sheets of hexagonal rings that look like chicken wire. Bacon's graphite whiskers were sheets of graphite rolled into scrolls, with the graphite sheets continuous over the entire length of the filament. Ultimately, it was replaced by more effective materials such as polyacrylonitrile and pitch. The carbon fibers weighed a fraction of the weight of steel yet contained much greater tensile strength than steel. Another important benefit of carbon fiber was its high modulus or resistance to stretching. This inelasticity plays an important role in reinforcing rigid structures such as the nose cones in hypersonic aircraft [2]. The United States Air Force and The National Aeronautics and Space Administration (NASA) didn't wait long to capitalize on carbon fiber technology. Stronger and lighter planes began to emerge as carbon fiber reinforced polymers (CFRPs) replaced heavy metals. These composites allowed aircraft to become faster and more efficient. Carbon fiber's high heat tolerance was also pivotal to building spacecraft that could withstand the intense heat at atmospheric re-entry.

Fibers have very interesting properties such as high length to diameter ratio and hence find a lot of applications in various industries. With advancement in technology and the introduction of nanotechnology, the production of nanometer-scale fibers (Nanofibers) in various scientific communities has attracted a lot of attention. These fibers possess a large surface area when compared with conventional fibers [3]. The incorporation of nanofillers into electrospun fibers enhances the fiber properties relevant to a number of applications, particularly mechanically reinforced composites. The important properties of the nanofibers, which make them commercially important are their small diameter, large surface area, and small pore size which are the ideal requirements for filtration, catalysis and adsorption. Large length to

diameter ratio and small mass to volume ratio of these nanofibers widens the areas of their application further.

Graphene a two dimensional allotrope of carbon discovered in 2004 [4,5] has attracted a lot of research interest due to its unique electronic structure and fascinating properties such as excellent optical, high thermal stable chemical and mechanical properties. Due to its excellent mechanical properties, graphene can be used in the formation of composite materials and reinforcement of fiber properties for improved performance. One of such properties includes thermal conductivity [6,7].

Electrospinning is one of the technique for production of continuous fibers from micro to nanometer range scale by the application of electrostatic forces to a jetting polymer solution [8]. The basic idea behind this technology dates back to the early 1950's [9–13]. Electrospinning is a very attractive technique in the production of nanoscale polymer fibers because of its simplicity, low cost, high productivity, reproducibility and its potential to be scaled up to the industrial scale [14]. Figure 1 shows histogram representing the number of scientific articles published in electrospinning and nanofiber per year during the last decade.

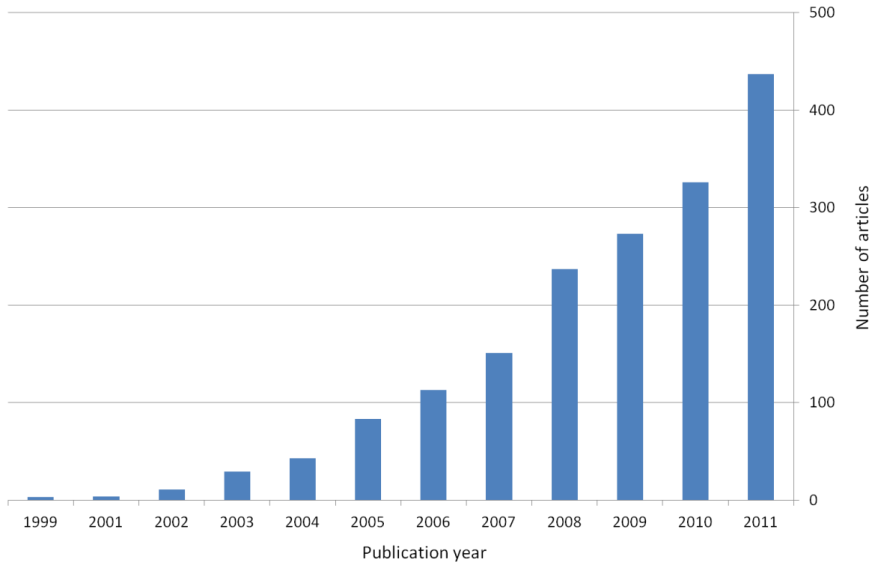

Figure 1. Histogram representing the number of scientific articles published per year during the last decade (Research performed on 4th June 2012 with "Web of Science", with "electrospinning" AND "nanofiber") [15].

Design of the polymeric nanofibers to meet specific needs for useful applications requires a thorough knowledge of the electrospinning parameters and their effect on nanofibers diameters and morphologies. [16,17]. The usual nanofillers include 0D nanoparticles [18], 1D nanotubes [19–21], 2D-layered materials [18,22,23] to improve the mechanical, electrical, thermal, and optical properties of the matrix. For the 2D-layered nanofillers, reduced graphene oxide (GO) [24,25] and graphene have provided very high performances to polymer based nanofibers due to high mechanical strength, electrical, and thermal conductivities [18,26,27] and making them best candidates for nanofillers. By adding graphene into the polymer, one can improve the mechanical [28,29], electrical [30] and thermal stability [27] of the polymer fibers.

In this dissertation polymer/graphene electrospun nanofibers are synthesized and characterized. Graphene used here is derived from three different starting materials which will be nano-fillers in Polyvinyl alcohol (PVA) which is one of the most industrially used polymer for various applications such in the aeronautics and space administration. The expectation is the improved mechanical and thermal properties of this polymer due to graphene inclusion. The increase of thermal stability even by 1 ^{0}C in polymer materials stability is extremely important.

This dissertation consists of five chapters with Chapter 1 being the general introduction, Chapter 2 will deal with literature review, Chapter 3 deals with the experimental procedures, while Chapter 4 is the discussion of the results and Chapter 5 deals with the conclusions and future work.

CHAPTER 2

LITERATURE REVIEW

2.1 CARBON AND GRAPHENE

Carbon is an exceptional element in the periodic table and plays a unique role in nature. Carbon has the ability to form very long interconnecting C-C bonds chains known as catenation. This ability allows carbon to form an almost infinite number of compounds by covalently bonding with other atoms or structures to create unlimited and extremely versatile compounds. This ability of carbon atoms to form complicated networks is fundamental to organic chemistry and the basis for the existence of life. Wide variety of compounds, including pharmaceutical and petroleum resins are a subset of organic carbon compounds. Physical and Chemical properties of carbon nanostructures play a unique and extensive role in the field of modern technology. The electron orbital in carbon atoms has the following electronic structure $1s^2 2s^2 2p^2$. So there are four free electrons, which can provide up to four bond with other atoms [31].

Carbon has five isotopes (C-11, C-12, C-13, C-14, C-15), two of which are very stable (C-12, C-13) while C-11 has a half-life of 20.3 minutes, C-14 has a half-life of 5730.0 years, and C-15 has a half-life of 2.5 seconds [32]. Carbon has many allotropes such as diamond, graphite, fullerenes and carbon nanotubes [6]. Graphene is a single flat layer of carbon atoms packed into honeycomb lattice and was discovered in 2004 [4,5] and is regarded theoretically as the

basis for the formation of all other sp^2 allotropes as shown in Fig. 2 below [33] where one can wrap graphene to produce 0D fullerene, roll it at certain axis to produce carbon nano-tubes and stack it to produce graphite. Graphite flakes consists of many graphene layers combined together by weak Van der Waals forces between them [34].

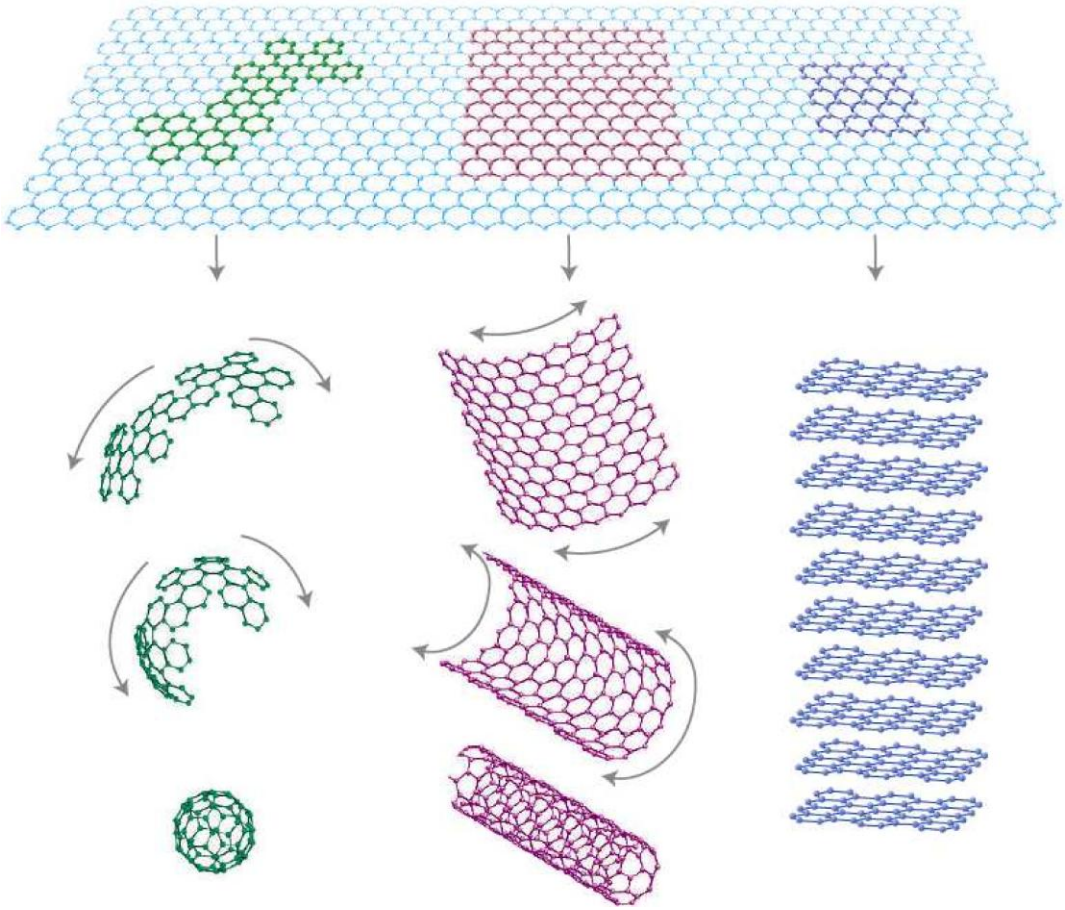

Figure 2. Graphene as the basic unit of 0D fullerene, 1D carbon nanotubes and 3D graphite[33]

A single layer of nanometers thick graphite (graphene) has a huge aspect ratios (Normally 200-1500), large surface area of about 2630 m^2/g, large Young's moduli (~ 1.00 TPa) and good thermal conductivity (3000 W/mK respectively) [35–37]. Because of all these interesting properties graphene sheets have become a very good alternative for fillers in polymer nano-composites. About 76 % increase in strength and a 62 % improvement of Young's modulus can be achieved by loading 0.7 wt. % Graphene-oxide (GO) to polymer materials [38]. A 60 % increase in strength and a 100% improvement of Young's modulus can also be achieved by loading 2.7 wt. % graphite [39].

2.2 POLYMER

If metals and inorganic compounds are set aside, polymeric materials comprise the rest of the world. The word polymer comes from the Greek word, "Poly" meaning many and "Meros" meaning unit or section. Polymers are super high molecular weight molecules, which are composed of repeating units [40,41]. They are mainly long chain molecules with repeating units called monomers that are covalently attached to each other. They can easily be molded into various complex shapes because they are strong, relatively inert and have low density [3].

Polymerization is a chemical reaction where simple molecule or monomer bonds with each other and creates huge molecule with large molecular weight [42]. The degree of polymerization (DP) is usually defined as the number of repeated units in the chain or the number of monomeric units in the polymer [41,42].

2.2.1 Classification of polymers

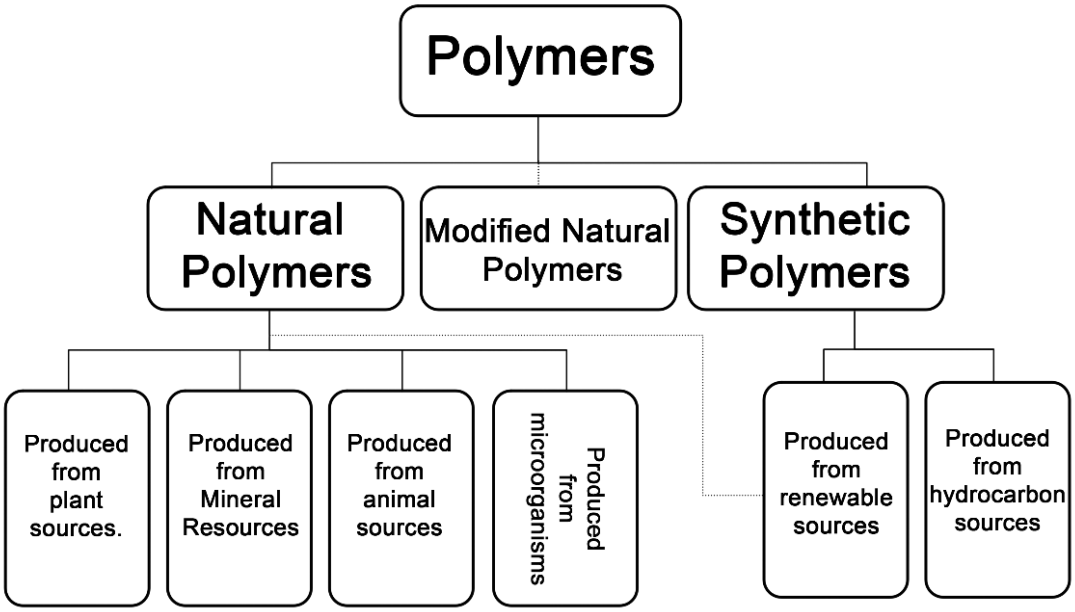

Figure 3. Classification of polymers based on origin [43–45]

Polymers are classified as either natural or synthetic (or modified natural), as shown in Figure 3 above. The natural polymers have been used for tens of thousands of years. The natural rubber was used by Olmecs at least 3000 years ago. In Egypt, papyrus was used for writing and styrene was used for embalming as far back as 3000 BC. Natural polymers are produced from plants (Cellulose, Starch, resin, etc.), minerals (Silicate, Asphalt, etc.), animal source (Chitin, Hyaluronic acid, etc.) or from microorganisms (Xanthan, Dextran, etc.).

The synthetic polymer refers equally well to linear, saturated macromolecules, unsaturated polymers, or to any substance based on cross-linked monomers, macromers, or pre-polymers and are product from hydrocarbon or renewable source [40,43,45,46].

We can classify the polymers based on their structure. Firstly, based on the type of monomers used, the following polymers are produced: Homopolymers (formed from only one type of monomer), and copolymers (the polymer contains at least two monomers). Secondly, based on the architecture or the shape, one can have the following polymer structures: linear, branched and cross-linked or networked.

They can also be classified based on their response to heat. Based on their abilities to melt, they can either be called thermoplastic or thermoset. Thermoplastic polymer (linear, branched–not cross-linked) can be melted or flows when heated and solidifies upon cooling. This heating and cooling can be repeated many times without affecting the properties of the thermoplastic polymer. Thermoset polymer that is cross-linked (with some exceptions) cannot melt or flow when heated. Heating this polymer leads to chain decomposition or bond breakage [3].

Finally, based on the morphology, we can have amorphous and semi-crystalline polymers. In an amorphous polymer the arrangements of the linear molecules is completely random and are intertwined like cooked spaghetti with a transparent appearance (glasslike). In a semi-crystalline polymer the molecules are packed together in ordered regions called crystallites and because these crystallites scatter light, they are more opaque [3,47].

2.2.2 Molecular Weight

The molecular weight of polymers is important because it determines many of its physical properties. Since virtually all polymers are mixtures of many large molecules, one must resort to averages to describe molecular weight. Among many possible ways of reporting averages, three are commonly used: the number average, weight average, and z-average molecular

weights. The weight average is probably the most useful of the three, because it fairly accounts for the contributions of different sized chains to the overall behavior of the polymer, and correlates best with most of the physical properties of interest [41]. A higher molecular weight increases the polymer's resistance to solvent dissolution [3].

2.2.3 Viscosity

The viscosity denoted by (η) is a parameter responsible for the frictional contribution of polymers in solutions. It is a physical property characterizing the resistance of fluids to flow. The viscosity of a polymer solution depends on concentration, size and molecular weight of the dissolved polymer [3,40,47,48]. If the solvent viscosity is η_0 and the viscosity of the polymer solution is η, the relative Viscosity is given by the expression below:

$$\eta_{rel} = \frac{\eta}{\eta_0}$$

The specific viscosity η_{sp} is the relative viscosity minus one:

$$\eta_{sp} = \eta_{rel} - 1$$

Usually η_{sp} is a quantity between 0.2 and 0.6. The intrinsic viscosity is given by:

$$[\eta] = \lim_{c \to 0} \left[\frac{\eta_{sp}}{C}\right]$$

Where C is a concentration and η is the viscosity

Mark–Houwink–Sakurada equation gives the relationship between the molecular weight and the intrinsic viscosity as follows:

$$[\eta] = KM_V^a$$

K and **a** are constants for a particular polymer–solvent pair at a particular temperature [47]. Table 1 shows the relationship between viscosity and molecular weight for some polymers.

Table 1. Viscosity and molecular weight relationship [47]

Polymer	**Solvent**	**T (°C)**	**K×10^3 [a]**	**a [b]**
Poly(vinyl acetate)	**Benzene**	**30**	**22**	**0.65**
cis-Polybutadiene	**Benzene**	**30**	**33.7**	**0.715**
Poly(ethyl acrylate)	**Acetone**	**25**	**51**	**0.59**
Polystyrene	**Butanone**	**25**	**39**	**0.58**
Polystyrene	**Cyclohexane (θ-solvent)**	**34.5**	**84.6**	**0.50**

[a] European units, concentrations in g/ml. Units do not very with a. Unit of **K** are $cm^3.mol^{1/2}/g^{3/2}$.

[b] The quantity **a**, last column, is the exponent in equation.

2.2.4 Glass Transition Temperature (T_g)

Glass transition temperature ($\mathbf{T_g}$) is sometimes confused with melting temperature ($\mathbf{T_m}$). Melting happens to crystalline polymers, while glass transition temperature only exits in amorphous polymers. $\mathbf{T_g}$ is the temperature range where a thermosetting polymer changes from a hard, rigid (glassy) state to a more pliable, compliant or rubbery state. Below $\mathbf{T_g}$, the amorphous polymer is brittle but above $\mathbf{T_g}$, cross-linked amorphous polymers exhibit rubber

elasticity [3,47,49]. Figure 4 shows the difference between glass transition temperature and melting point.

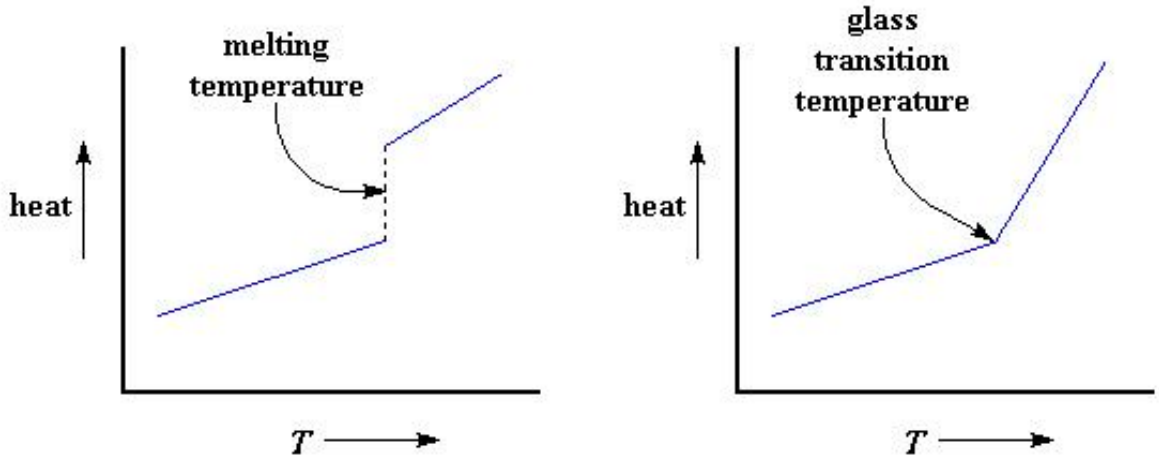

Figure 4 Difference between glass transition temperature and melting temperature [50]

2.2.5 Composites

Composite is a material that is made from two or more distinct material phases; a bulk phase (matrix) and a reinforcement phase. Usually the matrix is ductile or tough, while the reinforcements are strong with low densities [3].

Composite matrices consist of ceramic matrix composites (CMC), metal matrix composites (MMC) and polymer matrix composites (PMC) while composite reinforcements consist of fiber reinforced composite (FRC) and particle reinforced composites (PRC)

2.2.6 Example of some polymers

2.2.6.1 Polyvinyl acetate (PVAc)

In 1912, Dr. Fritz Klatte discovered polyvinyl acetate (PVAc) in Germany (Chemische Fabrik Griesheim). In the same year, he discovered polyvinyl chloride (PVC) [51]. The monomer of Vinyl is "CH=CH-" connected to the acetate "CH-COO" to produce PVAc "CHCOOCH=CH" with a molecular formula of $[C_4H_6O_2]_n$.

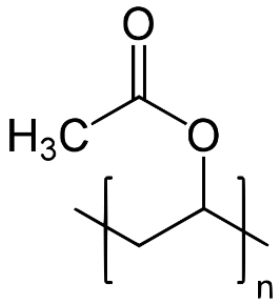

Figure 5. Structure of polyvinyl acetate

Its degree of polymerization is typically between 100 and 5000. The relative molecular mass lies between 10 000 and 1500 000 g/mol. The ester value, which characterizes the degree of hydrolysis, is between 615 and 675 [52–55].

2.2.6.2 Polyvinyl alcohol (PVA)

Polyvinyl alcohol (PVOH, PVA or PVAl) is produced commercially from polyvinyl acetate, usually by a continuous process. It has the molecular formula of $[C_2H_4O]_n$.

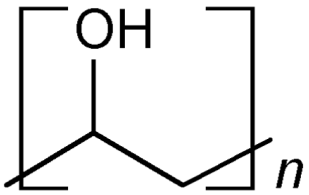

Figure 6. Structure of polyvinyl alcohol

PVA has a melting point of 230 ℃, density of 1.19 g /cm³ and its full hydroxylation occurs around 180–190 ℃. PVA is a water-soluble synthetic polymer. When dissolved in a solution, the viscosity of the solution increases [56,57].

2.2.7 Conductive polymer

Most polymers are electrically insulating. Not more than two decades ago, researchers found special polymers that are electrically conductive. The conductivity (σ) is expressed in unit of Siemens (S) per cm (S/cm) [58,59].

2.2.7.1 Polypyrrole (PPy)

Polypyrrole (PPy) is a conductive polymer formed by polymerization of pyrrole with iron (III) chloride [60]. The molecular formula and the reaction are respectively given by $[C_4H_2NH]_n$

$$nC_4H_4NH+2FeCl_3\rightarrow(C_4H_2NH)_n+2FeCl_2+2HCl$$

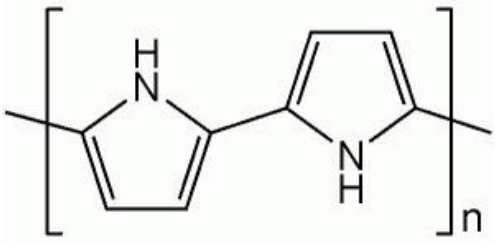

Figure 7. Structure of Polypyrrole

Polypyrrole has a molecular weight around 67,0892 g/mol, a melting point above 300 ℃ and does not dissolve in water [58,59,61–63].

2.3 CHEMICAL VAPOR DEPOSITION (CVD)

Chemical Vapor Deposition (CVD) was originally developed in the 1960s and 1970s and used in the production of carbon fibers and carbon nanofibers [64,65]. Figure 8 shows schematic of the CVD machine used in this study for synthesis of graphene.

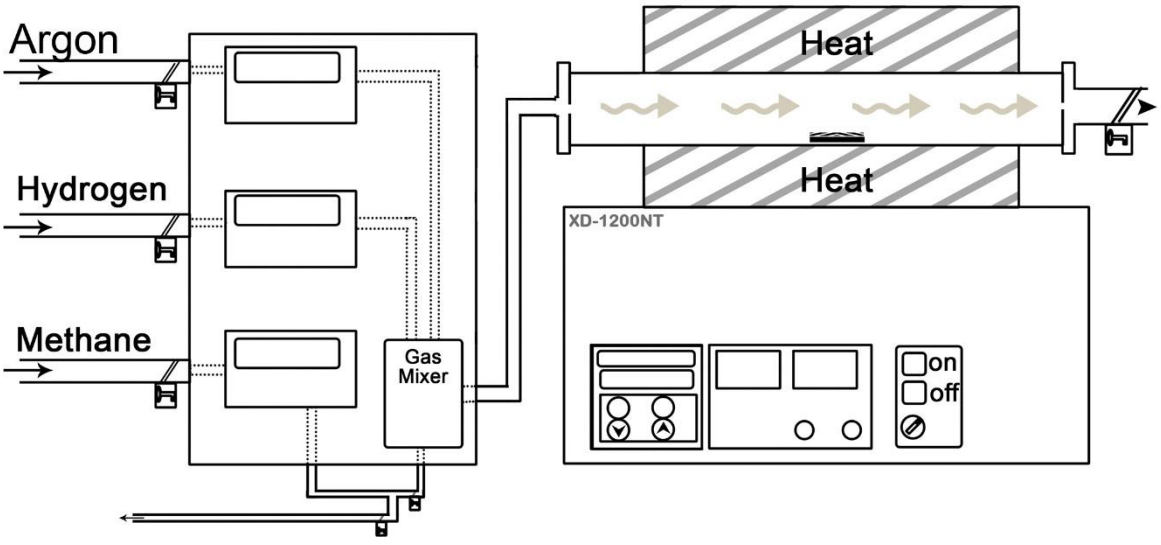

Figure 8. Schematic of the CVD machine used in this study

CVD is a process for depositing thin films of materials on substrates. Gas sources are introduced into the reaction chamber. Decomposition and reactions occur in the chamber at high temperature leading to film growth. CVD process can be used to deposit a wide range of conducting, semiconducting, and insulating materials [66]. Large area, high quality graphene can be grown by CVD on catalytic transition metal surfaces such as nickel and copper [64,67,68]. Methane (CH_4) is one of the commonly used carbon sources for the growth of high quality graphene. In this work, it was also used as the carbon source to grow graphene foam on Ni foam template.

2.4 NANOMATERIAL AND NANOFIBERS

2.4.1 Nanomaterial

The word nano comes from the Greek word (nannas) and means billionth i.e $1x10^{-9}$m. Nanomaterial is defined as particles of radius < 100 nm and/or their dimensions < the characteristic length of some phenomena (e.g. mean free path or scattering length - the distance travelled by e^- in the metal between collisions). Nanoscience is a field that deals with materials at the nanoscale by trying to understand their properties and influences. Nanotechnology is the understanding and control of matter at dimensions of roughly 1 to 100 nanometers, where unique phenomena enable novel applications. It encompasses nanoscale science, engineering and technology and involves imaging, measuring, modeling, and manipulating matter at this length scale.

2.4.2 Nanofibers

Fibers have high length to diameter ratio and hence they find many applications in various industries. With the advancement of technology and the advent of nanotechnology, nanoscale

fibers (Nanofibers) have attracted a lot of interest in various domains. These fibers provide a very large surface area compared to conventional fibers [3]. Polymeric nanofibers can be processed by a number of techniques such as drawing, template synthesis, phase separation, self-assembly and electrospinning [3].

2.4.2.1 Drawing

Drawing is one of the techniques that makes single nanofibers [8]. Drawing requires a pronounced viscoelastic material, cohesive enough to support the stresses developed during the pulling to undergo strong deformations. This method transforms the pulling material into a solid fiber [69]. Nanofibers can also be fabricated with citrate molecules by dipping a micropipette into a droplet and rapidly with drawing it [3]. This process is illustrated in Figure 9 below.

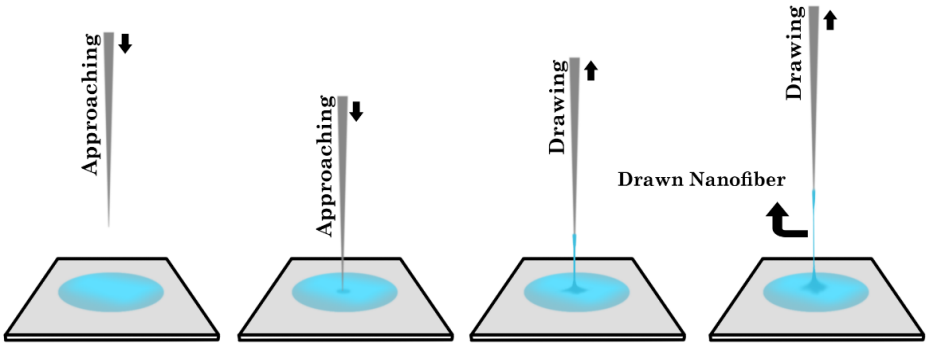

Figure 9. Drawing processes

2.4.2.2 Template synthesis

In template synthesis, polymer solution is placed in the holes of a template [3]. The template synthesis uses a nonporous membrane as a template. This method is not suitable for production of single continuous nanofibers [70]. Figure 10 shows template synthesis method.

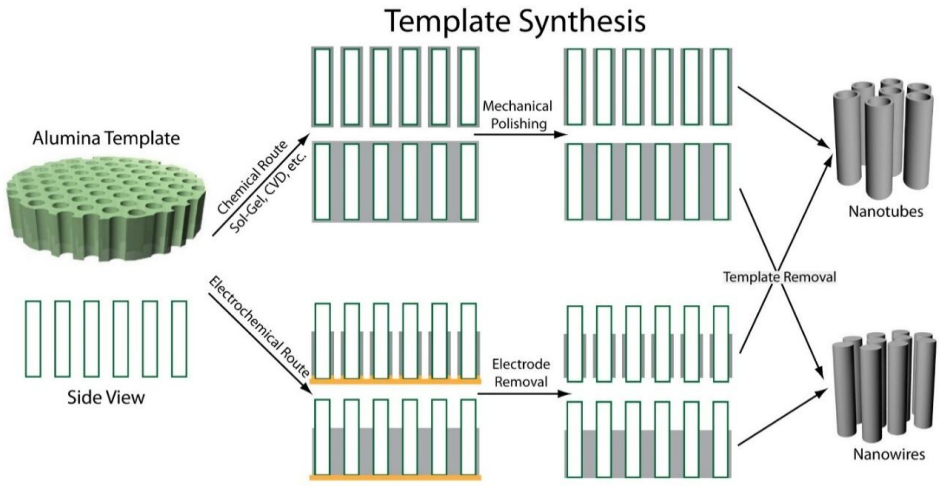

Figure 10. Schematic of production of nanofibers by template synthesis [71]

2.4.2.3 Phase Separation

In phase separation five steps are involved: dissolution of polymer, phase separation and gelation, extraction of solvent from the gel with water and freeze-drying under vacuum [3]. This technique cannot be used for the production of single continuous nanofibers. Figure 11 shows generic schematics of phase separation for obtaining nanofibrous structure.

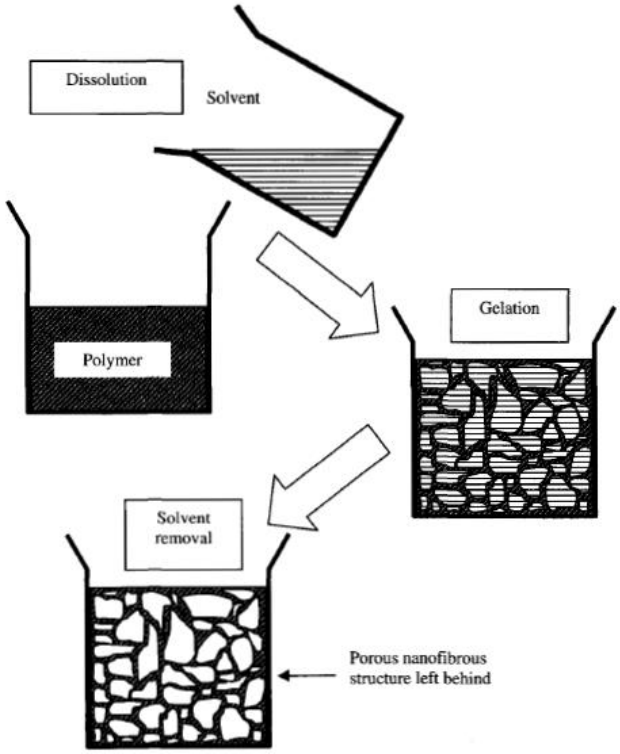

Figure 11. Generic schematic of phase separation for obtaining nanofibrous structure [3]

2.4.2.4 Self-assembly

Self-assembly of nanofibers makes use of smaller molecules to build nanoscale fibers [3,72]. This method can't give a very clear single nanofibers and are mostly used in biological application [72]. Figure 12 shows a simple schematic for self-assembly nanofibers growth.

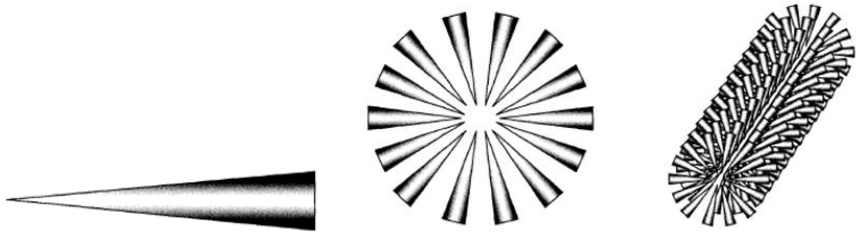

Figure 12. A simple schematic of self-assembly nanofibers [3]

2.5 ELECTROSPINNING

Electrospinning is one of the techniques used for production of continuous fibers from micro to nanometer range scale by the application of electrostatic forces to a jetting polymer solution [73]. This technique dates back to the early 1900 when Formhals published a series of patents [9–13]. He used an electrostatic force in an experimental setup for the production of polymer filaments. The polymer filaments were formed, from the solution between two electrodes. One of the electrodes was connected into the solution and the other connected to a collector [70]. Figure 13 shows Formhals patent images, process and apparatus for preparing artificial threads.

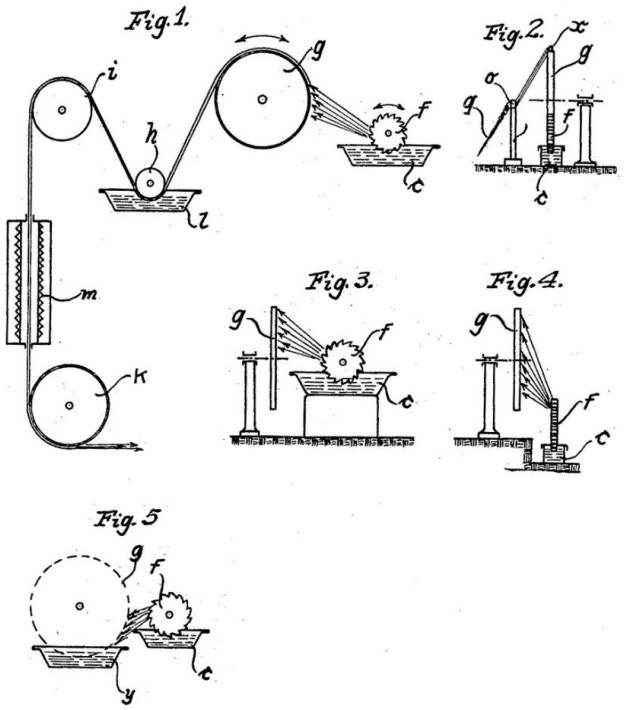

Figure 13. Formhals patent images, process and apparatus for preparing artificial threads [9]

Nanofibers from electrospinning have a lot of applications in industry and medicine. Today the electrospinning setup in its simplest form consists of high direct current (DC) voltage source to generate electric charge in the polymer solution, a cylinder to hold the polymer solution, a needle and collector [3]. Figure 14 shows the electrospinning setup in its simplest form.

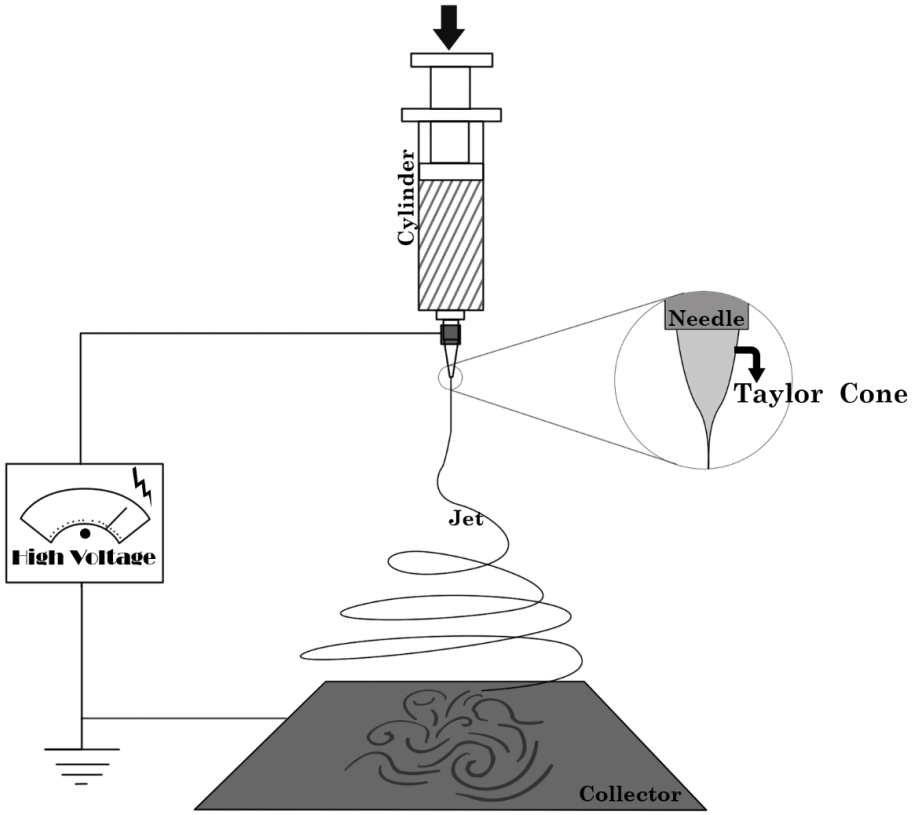

Figure 14. Electrospinning setup

2.5.1 Region

Electrospinning have four major regions namely the Taylor cone region, the steady jet region, the instability jet region (spraying region) and the collection region [74,75].

2.5.1.1 Taylor cone region

In a strong non-uniform electric field, a pendant drop will deform into a conically shaped volume of liquid. The conical formation occurs from a combination of charge repulsion and surface tension mechanisms. Figure 15 shows different forms of cone-jet mode that are due to different parameters such as an issued rate of flow (Q), the liquid properties density (ρ),

surface tension (σ), viscosity (η), electrical conductivity (K_e), electrical permittivity (ε_i) and the outer environment properties [76–80].

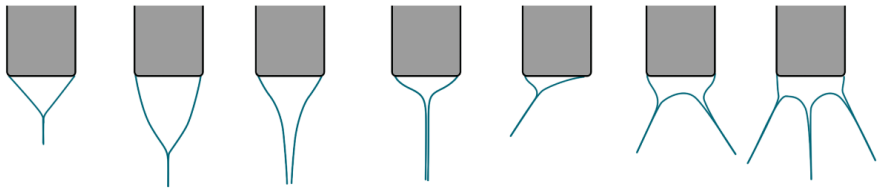

Figure 15. Different forms of cone-jet mode [78,79]

2.5.1.2 Steady jet region

The region after Taylor coin is the steady jet region. In this region, the liquid behaves like a jet and this jet possesses short diameter which is stable. The parameters that have effect on stable jet are balance of viscosity, charge density and surface tension. The terminal jet diameter is directly dependent on the flow rate, electric current, and surface tension of the fluid [81–83].

2.5.1.3 Instability jet region

Three main instabilities exists. These instabilities vary and increase with distance, electric field, and fiber diameter at different rates depending on the fluid parameters and operating conditions. The first instability is the Rayleigh instability at low electric fields, and is most dependent on the surface tension of the material. Two other instabilities arise with an application of higher electric fields and are dependent on the conductivity of the solution [81,82,84–86].

2.5.1.4 Collection region

In this region, different electrodes can be used for collection of the fibers. This collector can be a flat substrate or rotating drum. The collector has an effect on the morphology and can be modified to get aligned nanofibers in this region. Collectors used are usually conducting materials such as aluminum foil.[3,87].

2.5.2 Electrospinning parameters

In the electrospinning process some parameters have effects on the morphology, the diameter as well as the orientation of the electrospun fibers. Such parameters include the applied voltage, solution feed rate and the distance between needle tip and collector [88]. The morphology and diameter of the electrospun polymer fibers is dependent on many processing parameters. These parameters can be divided into three groups: (1) Solution properties, (2) processing conditions and (3) ambient conditions [3,89].

1. Solution properties: these properties include viscosity, polymer concentration, molecular weight of polymer, electrical conductivity, elasticity and surface tension

2. Processing conditions: the processing conditions are as follows: applied voltage, distance from needle to collector, volume feed rate and needle diameter

3. Ambient conditions: these include temperature and humidity.

2.5.2.1 Solution properties

The viscosity of the liquid jets is directly related to the solution concentration and the resultant fiber diameter. For less viscous solution the fiber usually contain beads. By

increasing the viscosity, average distance between beads becomes longer and the shape of beads changes from spherical to spindle. However, high viscosity may cause the failure of the electrospinning process because of flow instability. If the viscosity of the polymer liquid jet increases, the rate of solvent evaporation is reduced and the fiber diameter becomes larger. Molecular weight reflects the entanglement of polymer chains in solutions, namely the solution viscosity. Surface tension originates from the intermolecular force which tries to decrease the surface area per unit mass. In the electrospinning process, fibers can be produced without beads by reducing surface tension or increasing the viscoelastic force. Increasing the conductivity the electric force exerted on the jet produces thinner fibers [3,17,75,90].

2.5.2.2 Processing conditions

In electrospinning, when a voltage higher than threshold voltage is applied, the charges begin to be ejected from Taylor Cone. The effect of the electric force is to increase the surface area, opposing the formation of beads and making the jet diameter thinner [17,90,91]. The flow rate is a significant parameter. At lower flow rate the polymer solution will get enough time for polarization. If the flow rate is very high, bead fibers with bigger diameter will be formed rather than the smooth fiber with thin diameter owing to the short drying time prior to reaching the collector and low stretching forces [17,90–92]. Distance from needle to collector is another important parameter in electrospinning. If the distance is too short, the fiber will not have enough time to solidify before reaching the collector, whereas if the distance is too long, bead fiber can be obtained [93–95].

2.5.2.3 Ambient conditions

Ambient parameters such as temperature can also affect the fiber morphologies. Increasing temperatures give thinner fiber diameter. Low humidity may dry the solvent totally and increase the velocity of the solvent evaporation, while high humidity will lead to thick fiber diameter [96].

2.6 Characterization techniques

2.6.1 Raman Spectroscopy

Raman spectroscopy is a technique used to observe vibrational, rotational, and other low-frequency modes in a system. This analysis is non-destructive and can be used to estimate number of graphene layers, and also to check the quality of the graphene samples produced (defect density) [80,81]. Raman spectroscopic analysis of the graphene and polymer/graphene composites were performed using a T64000 micro-Raman spectrometer from HORIBA Scientific, Jobin Yvon Technology equipped with a triple monochromator system to eliminate contributions from the Rayleigh line. All the samples were analyzed with a 514 nm argon excitation laser with a 12 mW power at laser exit to avoid thermal effects. The analysis of the spectra was performed using LabSpec (Ver. 5.78.24) analytical software.

2.6.2 Morphology investigations

2.6.2.1 Scanning electron microscope (SEM)

The scanning electron microscope (SEM) uses a focused beam of high-energy electrons to generate a variety of signals at the surface of solid specimens. The signals that derive from

electron/sample interactions reveal information about the sample including external morphology (texture), chemical composition and orientation of materials making up the sample [97]. The surface morphology of all samples was investigated using a Zeiss Ultra Plus 55 field emission scanning electron microscope (FE-SEM). "Image J" was used to measure the diameter of fibers from SEM images.

2.6.3 Thermal measurements

Thermogravimetric analysis (TGA) was performed in an Instrument Specialist system to determine the thermal stability of the fiber mats.

2.6.3.1 Thermo gravimetric Analysis (TGA)

Thermogravimetric analysis (TGA) (TA Instruments Q600 Simultaneous DSC/TG) measures the weight change in a material as a function of temperature (or time) under a controlled atmosphere [98]. Inorganic materials, metals, polymers, plastics, ceramics, glasses, and composite materials can be analyzed with TGA. TGA samples were heated from room temperature to 1000^{o}C at a rate of 10^{o}C min^{-1} in air.

CHAPTER 3

MATERIALS AND EXPERIMENTAL METHODS

This chapter introduces the materials that were used and experimental procedures which include graphene synthesis, preparation of polymer solutions, preparation of polymer/graphene solutions and the electrospinning procedure of the prepared solutions.

3.1 MATERIALS

The following materials were used in this study: Nickel foam (Alantum, Munich, Germany), pure graphite rod (s-01685-FA SPI Supplies Division), expandable graphite (grade ES 250 B5) from Qingdao Kropfmuehi Graphite, Polyvinyl alcohol (PVA) (M_w 89,000–98,000 g mol^{-1}) 99+% hydrolyzed (341584), Hydrogen (H_2), argon (Ar) and methane (CH_4) gases (all from Afrox).

3.2 SYNTHESIS OF GRAPHENE FOAM BY CHEMICAL VAPOR DEPOSITION (CVD) METHOD

Graphene foam (GF) was synthesized using CVD system as reported in reference [99]. Nickel foam substrate with 420 g/m^2 in area density and 1.6 mm in thickness was used as a template for the growth of graphene. Briefly, the nickel foam was annealed at 800 ℃ in the presence of

Ar and H_2 for 20 minutes to remove impurities, before the introduction of the CH_4 gas at 1000 ℃. The flow rates of the gases (CH_4:H_2:Ar) were 10:10:300 sccm. After 15 minutes of deposition, the sample was rapidly cooled by pushing the quartz tube to a lower temperature region. After growth, the nickel template was removed by chemical means. Briefly, polymethylmethacrylate (PMMA) was coated on the sample and baked at 180 ℃ for 30 minutes, in order to provide support and maintain the three dimensional shape of the graphene foam during etching of nickel. The sample was then placed in 3 M HCl solution at 80 ℃ and left overnight to ensure complete removal of the nickel. The resulting graphene foam sample was placed in acetone at 80 ℃ for 5 hours to completely remove the PMMA, further placed in isopropanol at 80 ℃ for 1 hour to remove the acetone and finally rinsed in deionized water to remove isopropanol. A subsequent annealing was performed at 400 ℃ in Ar. After the annealing process, the sample was again rinsed in deionized water and dried at 50 ℃ in an electric oven.

3.3 EXFOLIATION OF GRAPHITE

For synthesis of exfoliated graphite samples, expandable graphite was put in a quartz boat and placed in a microwave oven for irradiation to produce expanded graphite (EG), while pure graphite rods were grounded into powder form for sample preparation.

3.4 THE PREPARATION OF PVA SOLUTIONS

PVA solutions were prepared by dissolving PVA in deionized water in an Erlenmeyer flask in which the temperature was maintained at 80-90 ℃ and a magnetic stirrer was used for 3 hours. The viscosity of the PVA solution is dictated by the polymer concentration. In other

words, the higher the concentration of PVA, the more viscous is the solution. Table 2 shows the preparation of the PVA solutions with different concentrations and the viscosity measurement of the PVA solutions with different concentrations is shown in Figure 16 which clearly shows that viscosity increases with PVA concentration.

Table 2. Preparation of the PVA solution with different concentrations

Solution No	**PVA Weight (g)**	**Distilled Water (ml)**	**PVA Solution Concentration (wt. %)**
1	**3.47**	**40**	**8**
2	**4.44**	**40**	**10**
3	**5.45**	**40**	**12**

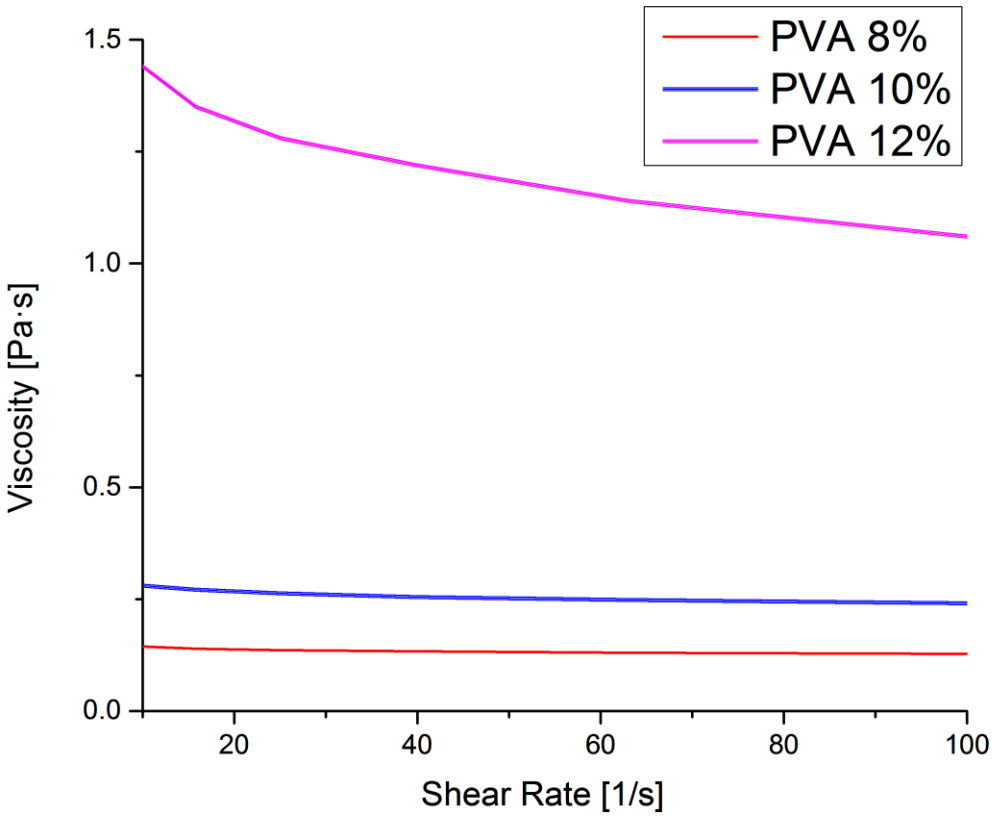

Figure 16. Viscosity measurement of the PVA solutions with different concentrations

3.5 THE PREPARATION OF GRAPHENE/PVA SOLUTIONS

For preparation of the solution, the GF was ultrasonicated in the PVA solution to obtain a good dispersion of graphene sheets. The solution was tip sonicated using a Eumax sonicator (ud100sh) for 5 hours at 40 ℃. The dispersion was then centrifuged at 5000 rpm for 3 minutes to remove aggregates of the remaining three dimensional network of graphene. EG was also ultrasonicated in the PVA solution in order to get graphene sheets[16]. Stable graphene dispersions were prepared by loading EG in the PVA solution after ultrasonication. The

solution was tip sonicated for 5 hours at 40 ℃. The dispersion was then centrifuged at 5000 rpm for 3 h to remove aggregates [16]. Similar steps were employed for pure graphite powder (G powder) to produce solutions for electrospinning. In this method, the non- exfoliated graphite aggregates can be easily removed after centrifugation because they are heavier than exfoliated graphene sheet dispersed in the PVA solution. Tables 3, 4 and 5 show the solutions prepared with different mass of graphene foam, graphene from EG and graphite powder, respectively.

Table 3. The PVA/graphene foam solutions at different GF concentrations

Solution No	**graphene foam Weight (g)**	**PVA Solution (ml)**	**PVA Concentration (wt. %)**
4	**0.02**	**10**	**10**
5	**0.04**	**10**	**10**
6	**0.06**	**10**	**10**
7	**0.08**	**10**	**10**

Table 4. The PVA/graphene derived from expanded graphite solutions at different expanded graphite concentrations

Solution No	expanded graphite Weight (g)	PVA Solution (ml)	PVA Concentration (wt. %)
8	0.02	10	10
9	0.04	10	10
10	0.06	10	10
11	0.08	10	10

Table 5. The PVA/graphene derived from graphite powder solutions at different graphite powder concentrations

Solution No	graphite powder Weight (g)	PVA Solution (ml)	PVA Concentration (wt. %)
12	0.02	10	10
13	0.04	10	10
14	0.06	10	10
15	0.08	10	10

3.6 ELECTROSPINNING

For electrospinning, standard NaBond electrospinning machine was used. The solution was loaded into a hypodermic syringe (10 ml) and a flexible tube was used to connect the syringe to the blunt needles (Gauge 6). A syringe pump (NaBond Technologies SN -50F6) was used to control the flow rate of the solution which was varied between 3 and 7 ml/h. The applied voltage between the needle and the collector was adjusted between 10 and 30 kV. Fibers were collected on a rotating collector (NaBond Technologies 150~6000 rmp) with the distance from the needle to the collector being varied between 10 and 14 cm. The rotating collector speed was also varied between 500 to 1000 rmp. The fiber growth time varied from 30 to 180 seconds. Glass (18 x 18 mm) (‘Cover glasses’ thickness No. 1 from Marienfeld) was used as substrate to collect the fibers. The substrate was stacked to the collector by conductive tape. After setting up the syringe pump and filling the syringe with solution, the latter is connected to the blunt needle and the needle is similarly connected to the applied voltage. Figure 17 is the schematic of the electrospinning machine used in this work.

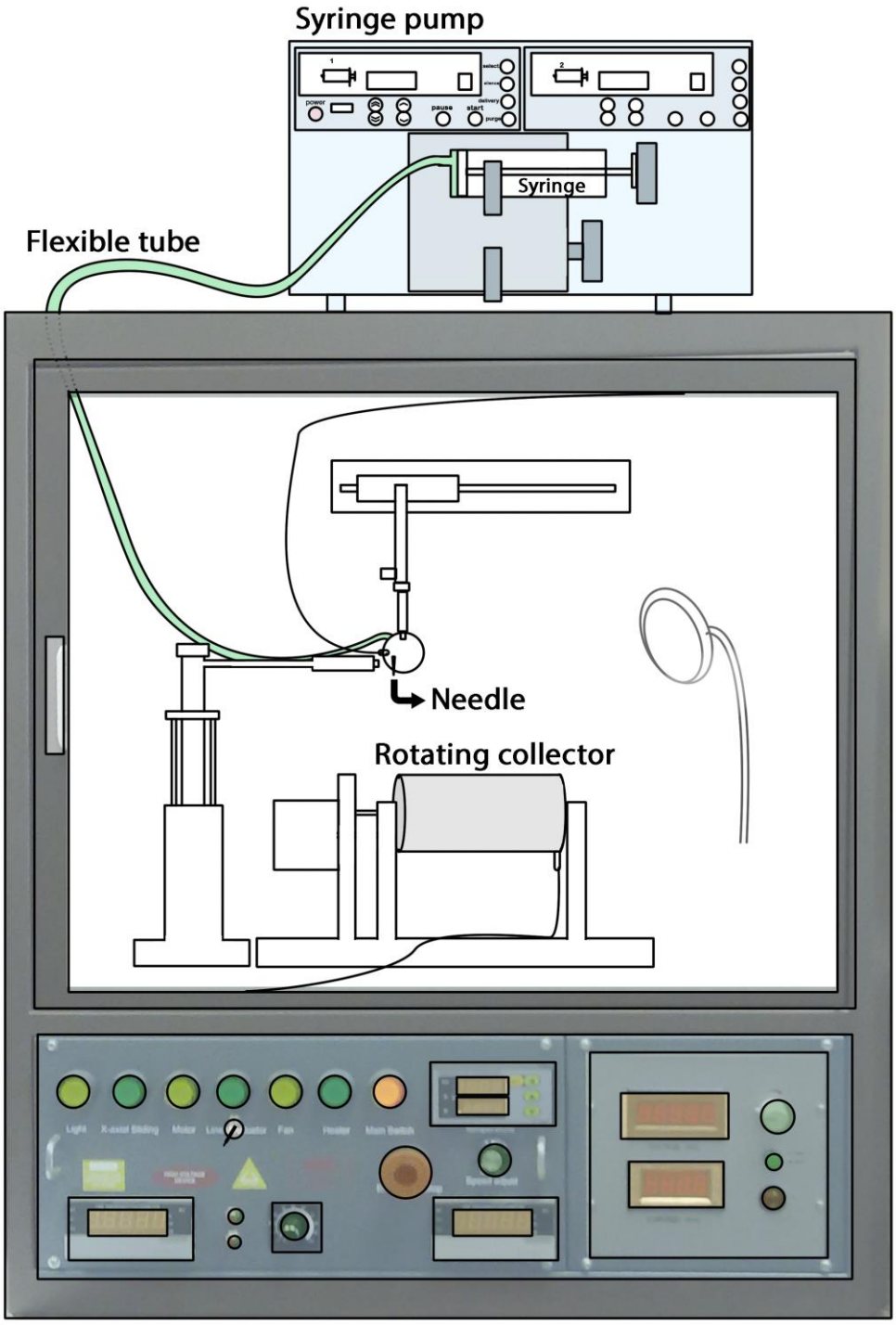

Figure 17. Schematic of Electrospinning machine used for fibers growth.

CHAPTER 4

RESULTS AND DISCUSSION

4.1 ELECTROSPUN PVA NANO-FIBER MORPHOLOGY

The morphologies of the PVA fibers, like all the fibers grown in this work, can be controlled by different parameters; polymer concentration, flow rate, applied voltage, duration of electrospinning and distance between needle tips to collector.

4.1.1 Effect of Solution Concentration

The fibers morphology and diameter can be modified by changing the concentration of the polymer solution. Sample 1 (S1), Sample 2 (S2) and Sample 3 (S3) with different concentrations of 8 wt.%, 10 wt.%, and 12 wt.%, respectively, shown in Table 2, were used for electrospinning of PVA fibers and their morphology were examined using SEM. Table 6 shows the different solution concentration of PVA used for fiber synthesis while the other parameters were kept constant . Figure 18 shows SEM images of the different samples labeled S1, S2 and S2 respectively.

Table 6. PVA concentration used for the growth of PVA fibers

Sample No.	PVA Concentration (wt.%)	Flow rate (ml/h)	Applied voltage (KV)	Time (s)	Distance (cm)	Speed (rpm)
S1	**8**	**3**	**30**	**60**	**12**	**1000**
S2	**10**	**3**	**30**	**60**	**12**	**1000**
S3	**12**	**3**	**30**	**60**	**12**	**1000**

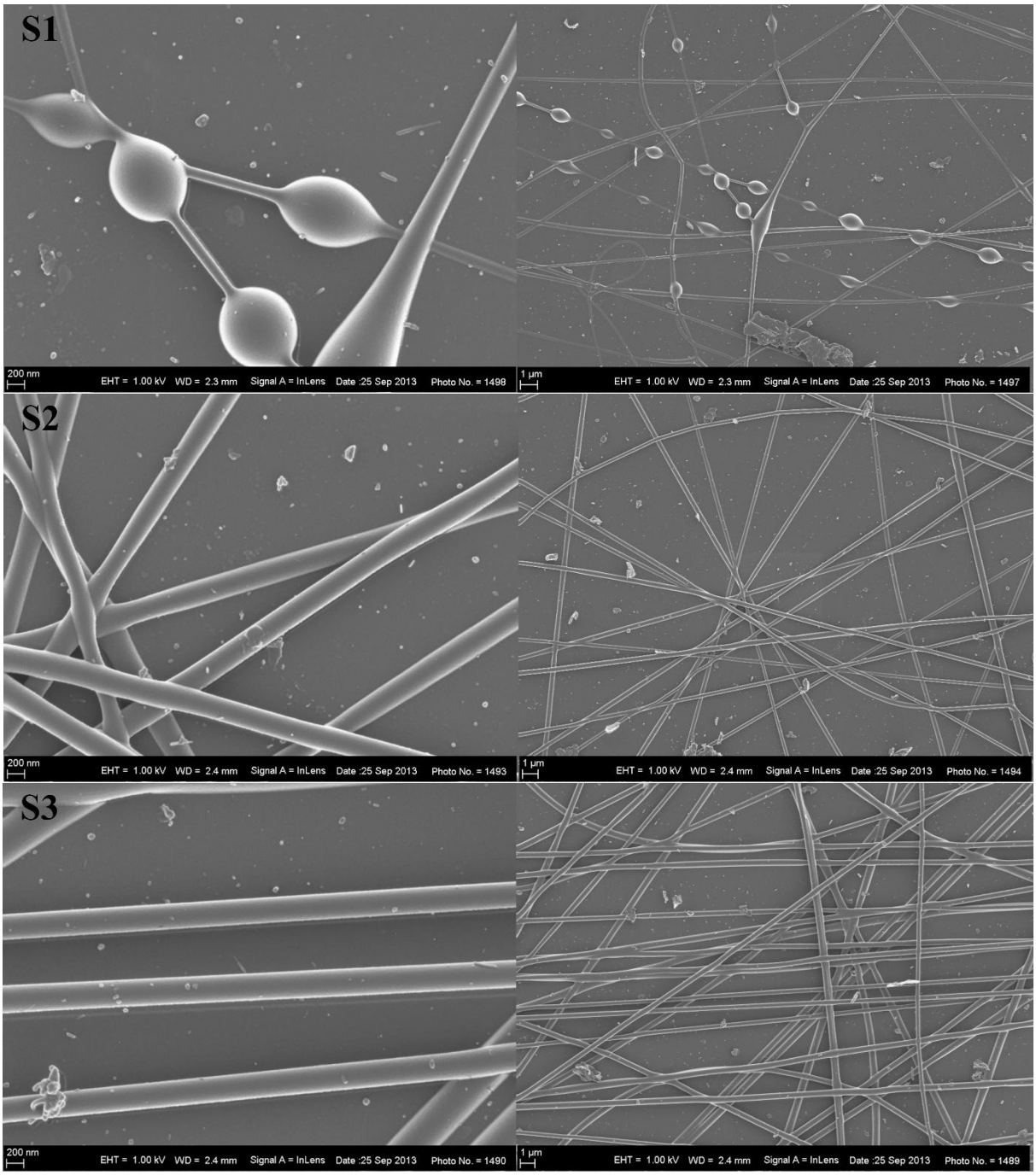

Figure 18. SEM micrographs of S1 (8 wt.% PVA concentration), S2 (10 wt.% PVA concentration) and S3 (12 wt.% PVA concentration) as described in Table 6 at different scales of 200 nm on the left and 1 µm on the right

As discussed before (Section 2.4.2.1), the viscosity of the polymer solution is an important parameter in the electrospinning process and the resulting fiber morphology. When the solution containing 8 wt.% of PVA was used (S1), the diameter of the fibers were thinner than the other two solutions but with high density of beads and drops in the fibers. The appearance of beads and droplets in the electrospun fibers is signature of instability in the solution and hence it is clear from these results that S1 was not a good sample to be used for synthesizing good continuous fibers. This beads and drops disappeared with increasing viscosity of the electrospun solutions (S2 and S3). For these two solutions, thicker fibers were obtained. In other words, the fiber diameters increase with increasing PVA concentration or solution viscosity. These results show that relatively high viscous solution is needed to avoid formation of beads and drop without comprising too much the diameter of the fibers. Due to the observation stated here 10 wt% of PVA solution will be used throughout this study. Table 7 summarizes the diameters of the fibers obtained with different concentration of PVA using 'Image J' software.

Table 7. Average diameter of fibers with different PVA concentration

Sample NO.	**PVA Concentration (wt.%)**	**Fiber Diameter (nm)**	**Fiber Morphology**
1	**8**	**121 - 264**	**Uniform thin fibers with beads**
2	**10**	**292 - 301**	**Thinner and smoother**
3	**12**	**295 - 440**	**Thicker and smoother**

4.1.2 Effect of flow rate

The fiber morphology can also be modified by changing the flow rate of electrospun solution. Different flow rates together with other fixed parameters are shown in Table 8 with corresponding samples labeled S4, S5 and S6. The corresponding SEM results are shown in Figure 19. Table 9 shows the average diameters of fibers obtained with different flow rate of the electrospun PVA solution.

Table 8. Varied flow rate of Electrospun PVA fibers

Sample NO.	PVA Concentration (wt.%)	Flow rate (ml/h)	Applied voltage (kV)	Time (s)	Distance (cm)	Speed (rpm)
S4	**10**	**3**	**30**	**60**	**12**	**1000**
S5	**10**	**5**	**30**	**60**	**12**	**1000**
S6	**10**	**7**	**30**	**60**	**12**	**1000**

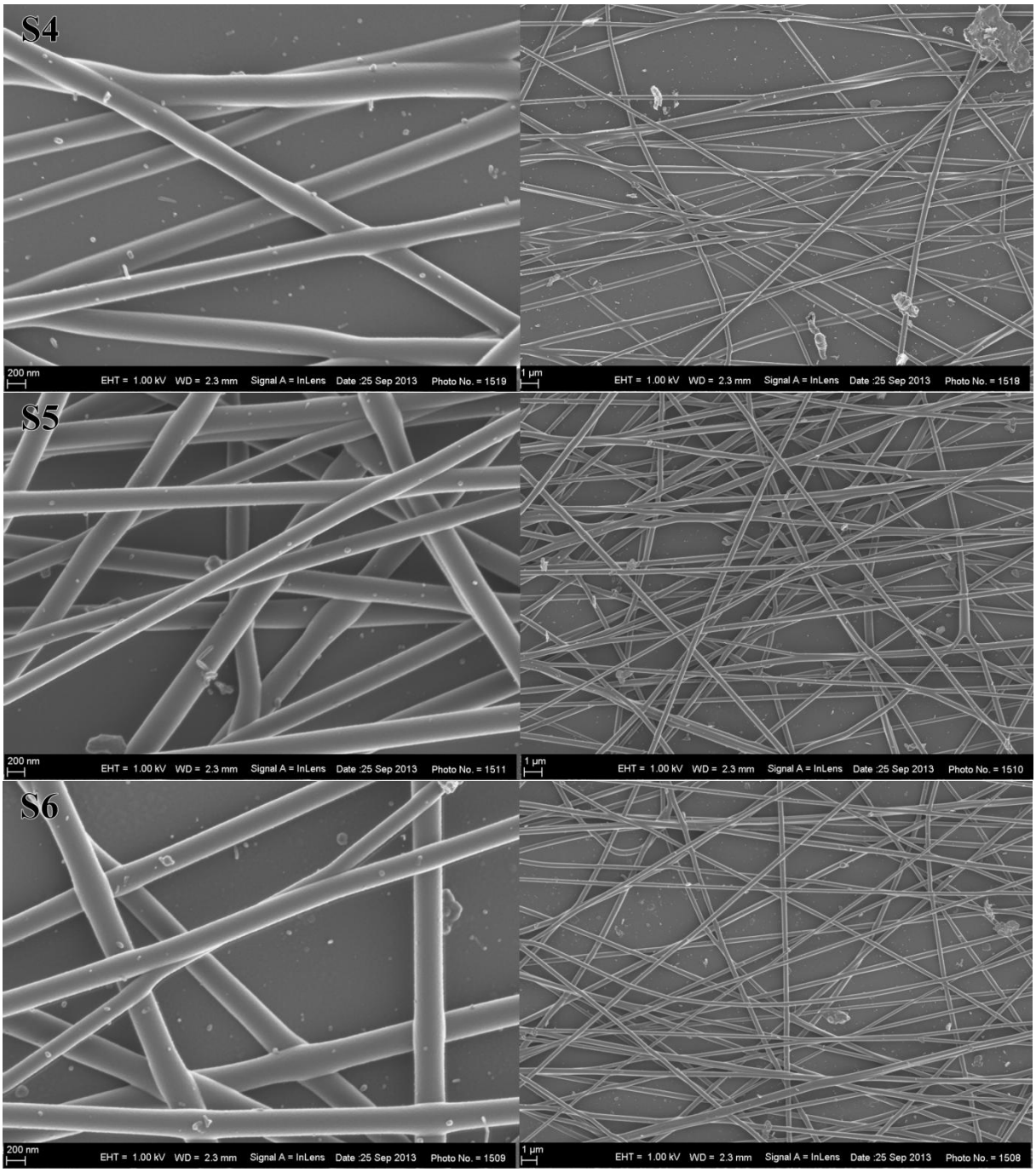

Figure 19. SEM micrographs of samples S4 (3 ml/h flow rate), S5 (5 ml/h flow rate) and S6 (7 ml/h flow rate) as shown in Table 8 at different scales of 200 nm on the left and 1 µm on the right

Table 9. Average diameter of fibers obtained with different flow rate

Sample NO.	Flow rate (ml/h)	Fiber Diameter (nm)	Fiber Morphology
4	**3**	**238 - 302**	**Thinner fiber**
5	**5**	**244 - 317**	**Thicker fiber with drop**
6	**7**	**270 - 333**	**Thicker fiber with drop**

It is observed that higher flow rates produce thicker fibers with some droplets. Increasing the flow rate will deliver more PVA solution to the Taylor cone, which increases the diameter of the liquid jet, resulting in the formation of thicker fibers. Furthermore, with further increase in PVA solution flow rate, the Taylor cone starts to decay and the continuous flow of solutions turns into discrete drops. It is then decided that low flow rate of 3 ml/h will be used as optimized one throughout this study.

4.1.3 Effects of applied voltage

The applied voltage between the needle and the collector plays an important role that influences the morphology and diameter of the resulting fibers. In this part, three different voltages were applied and the corresponding samples are labeled S7 for 10 kV, S8 for 20kV and S9 for 30 kV. Table 10 recapitulates the different parameters used in this section. Figure 20 shows the SEM images of the fibers grown under these conditions.

Table 10. Electrospinning setup with different applied voltage

Sample NO.	PVA Concentration (wt.%)	Flow rate (ml/h)	Applied voltage (kV)	Time (s)	Distance (cm)	Speed (rpm)
S7	**10**	**3**	**10**	**60**	**12**	**1000**
S8	**10**	**3**	**20**	**60**	**12**	**1000**
S9	**10**	**3**	**30**	**60**	**12**	**1000**

When increasing the applied voltage from 10 to 30 kV, the diameter of the fibers decreases (see Table 11). Increasing the applied voltage enhances the magnitude of the electric field which results in thinner liquid jet. When the applied voltage decreases, the fiber diameter increases and the core of the fiber stays liquid, so when it arrives at the collector, the resulting fiber is deformed. The SEM images and tabulated results in Table 11 show that 30 kV applied voltage produced much better fibers and hence will be used throughout this work.

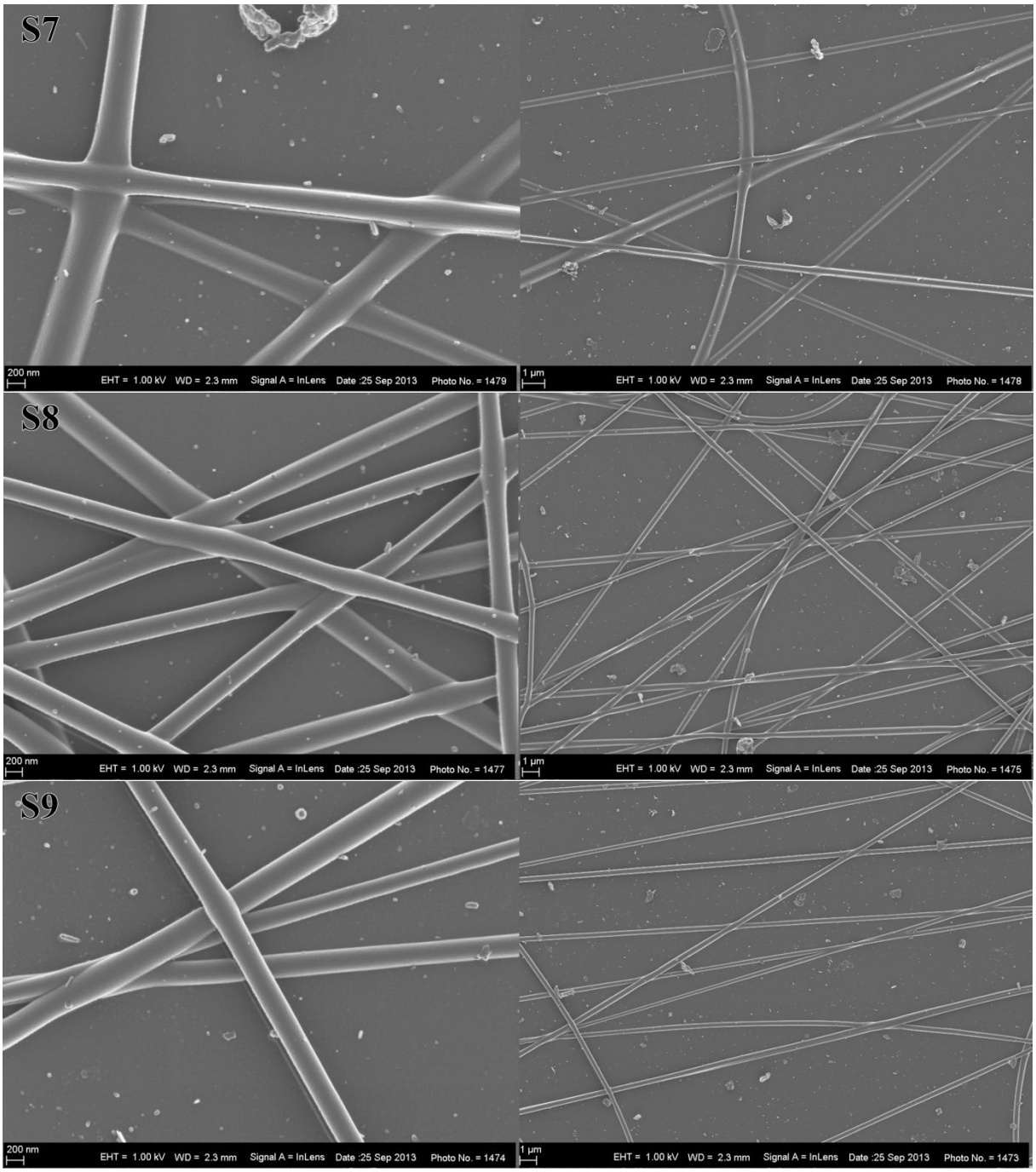

Figure 20. SEM micrographs of S7 (10 kV applied voltage), S8 (20 kV applied voltage) and S9 (30 kV applied voltage) as described in Table 10 at different scales of 200 nm on the left and 1 µm on the right

Table 11.Average diameter of fibers at different applied voltage

Sample NO.	Applied voltage (kV)	Fiber Diameter (nm)	Fiber Morphology
S7	**10**	**274 - 523**	**Thicker fiber and deformed**
S8	**20**	**250 - 417**	**Thinner fiber**
S9	**30**	**190 - 346**	**Thinner fiber**

4.1.4 Effect of time for electrospinning

The effect of electrospinning time on the morphology of the fiber was also studied. Three samples were prepared at different times as S10, S11 and S12 which correspond to electrospinning time of 30, 60 and 90 seconds respectively as shown in Table 12. The resulting fibers were examined using SEM (Figure 21) and Table 13 shows the average diameter of the fibers at different growth times.

Table 12. Electrospinning setup with different growth time

Sample NO.	PVA Concentration (wt.%)	Flow rate (ml/h)	Applied voltage (kV)	Time (s)	Distance (cm)	Speed (rpm)
S10	**10**	**3**	**30**	**30**	**12**	**1000**
S11	**10**	**3**	**30**	**60**	**12**	**1000**
S12	**10**	**3**	**30**	**90**	**12**	**1000**

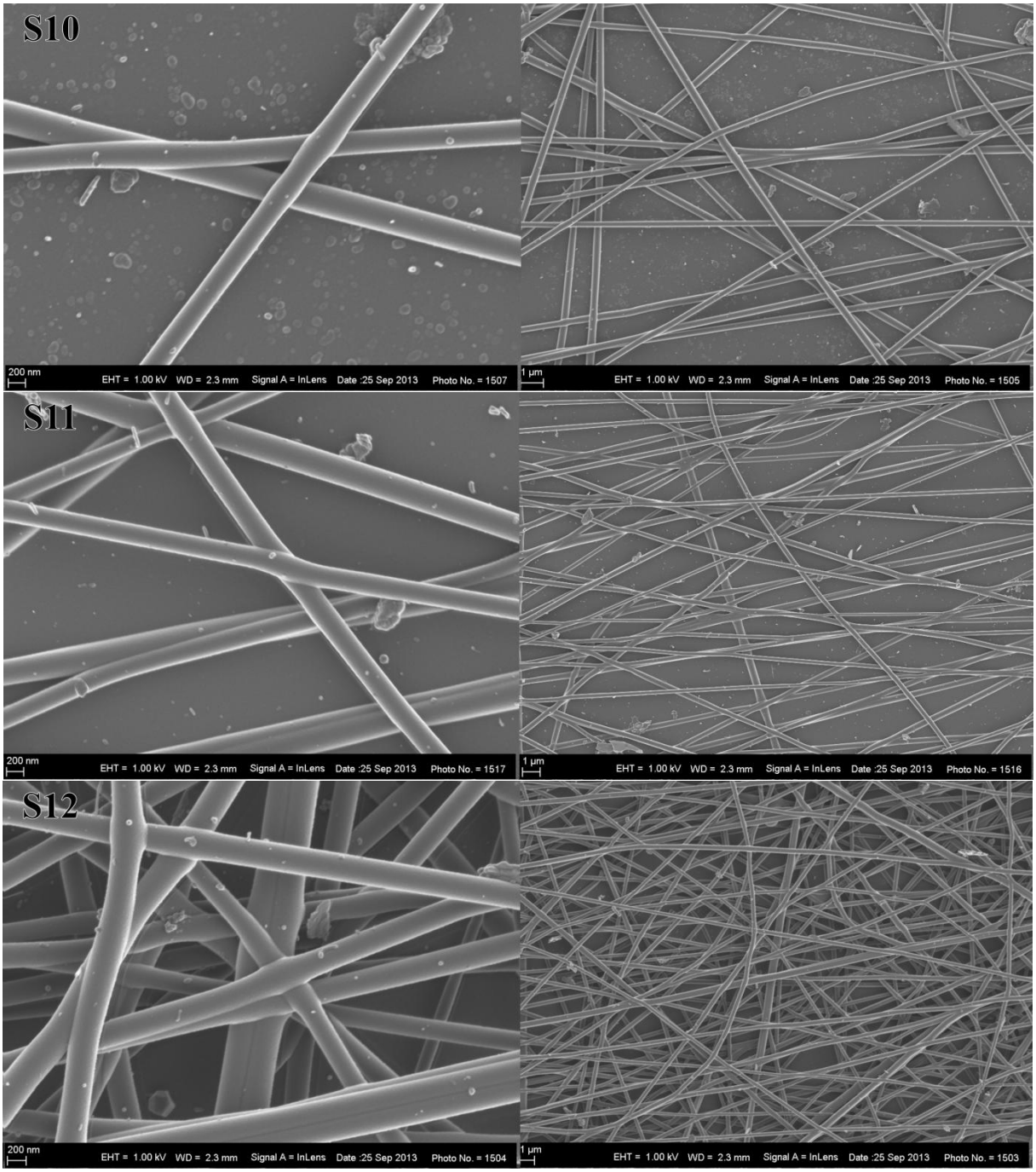

Figure 21. SEM micrographs of S10 (30 s growth times), S11 (60 s growth times) and S12 (90 s growth times) described in Table 12 at different scales of 200 nm on the left and 1 µm on the right

Table 13. Average diameter of fibers at different growth times

Sample NO.	Time (s)	Fiber Diameter (nm)	Fiber Morphology
S10	**30**	**271 - 361**	**Thinner**
S11	**60**	**200 - 336**	**Thinner**
S12	**90**	**275 - 465**	**Thicker at top**

Here it is observed that diameter of the fibers increases with the increasing growth time which in principle should not have any influence on the diameter of fibers. This effect is common for non-conductive polymers like PVA used in this work. In fact, the non-conductive polymer can cover up the surface of the collector and therefore directly affecting the voltage between the needle and the collector. Consequently, the fibers on top tend to be thicker. In this study 60 seconds time was considered to be the best growth time for the fibers because of the range of diameter of the fibers produced and will be used throughout this work.

4.1.5 Effect of distance between the needle tips and the collector

The distance between the needle tips and the collector must also be set to a singular golden distance to obtain the best fibers. Three different distances were investigated here with such samples labeled S13, S14 and S15 for distances of 10, 12 and 15 cm between the end of the needle and the collector, respectively, as shown in Table 14 below. The SEM images and the corresponding diameter dependence on distance are shown in Figure 22 and Table 15, respectively.

Table 14. Experimental setup with different distance between the needle tip and the collector

Sample NO.	PVA Concentration (wt.%)	Flow rate (ml/h)	Applied voltage (kV)	Time (s)	Distance (cm)	Speed (rpm)
13	**10**	**3**	**30**	**60**	**10**	**1000**
14	**10**	**3**	**30**	**60**	**12**	**1000**
15	**10**	**3**	**30**	**60**	**14**	**1000**

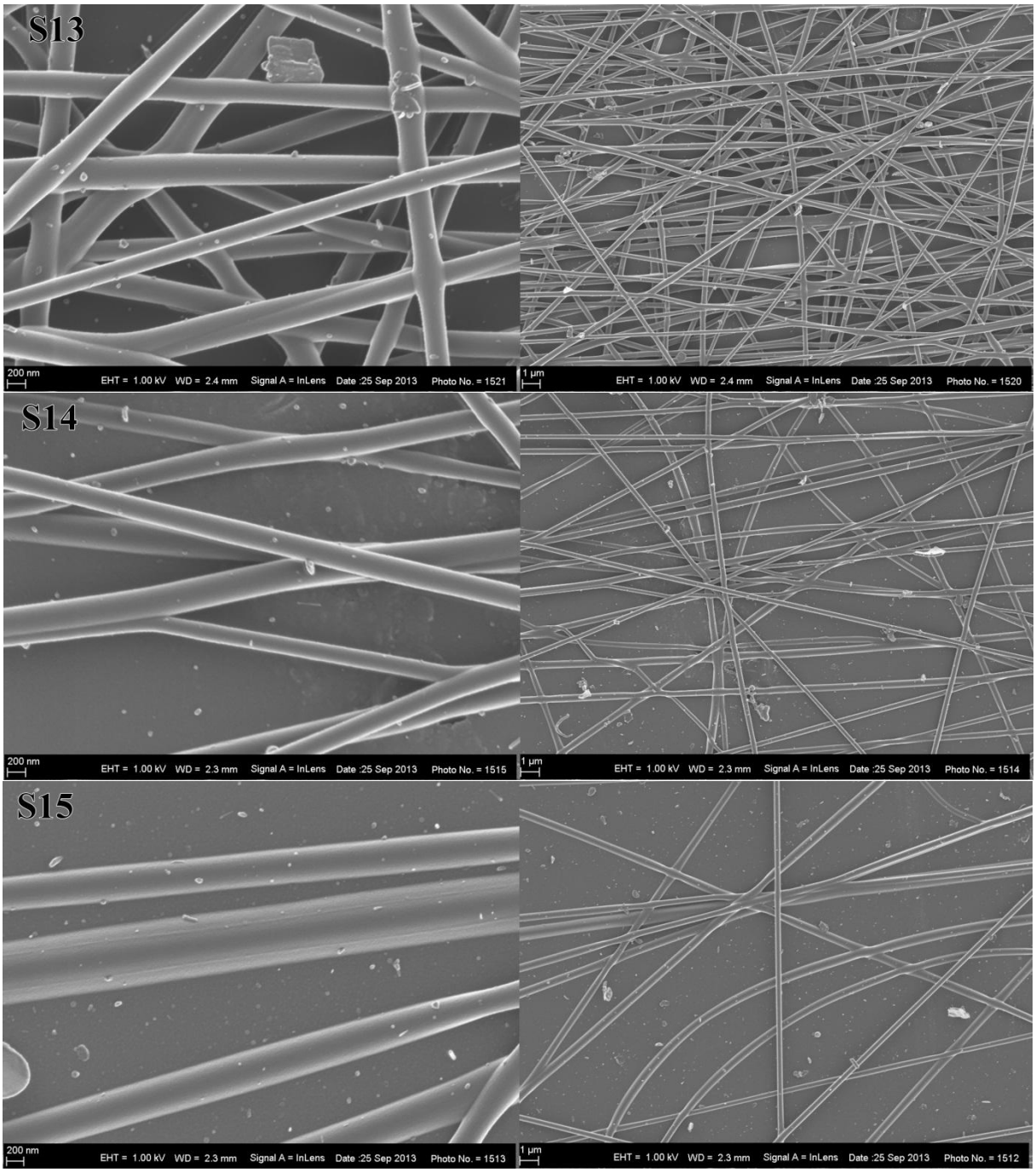

Figure 22. SEM micrographs of S13 (distances of 10 cm), S14 (distances of 12 cm) and S15 (distances of 14 cm) as described in Table 14 at different scales of 200 nm on the left and 1 µm on the right

Table 15. Average diameter of fibers with different distance between the needle tips and the collector

Sample NO.	Distance(cm)	Fiber Diameter (nm)	Fiber Morphology
13	**10**	**221 - 330**	**Thinner**
14	**12**	**199 - 313**	**Thinner**
15	**14**	**416 - 738**	**Thicker**

The distance from the needle tips to the collector has to be set to a golden distance in order to produce thinner fibers, because any distance below or above this golden distance will result in larger fiber diameter. This is due to the fact that if the distance is too short, the fibers will not have enough time to dry and the fiber diameter increases, while on the other hand when the distance is too long the effect of voltage on the liquid jet will be small and hence results in much thicker fibers. In this work it was observed that 12 cm is such a golden distance to produce good fibers and it will be used throughout.

Furthermore, for electrospinning of hollow nanofibers have been produced before using different methods [100,101]. In this study the hollow fibers were just produced through optimization of electrospinning parameters as shown in Figure 23 clearly showing that it will be possible to put some fillers in the fibers such as graphene flakes.

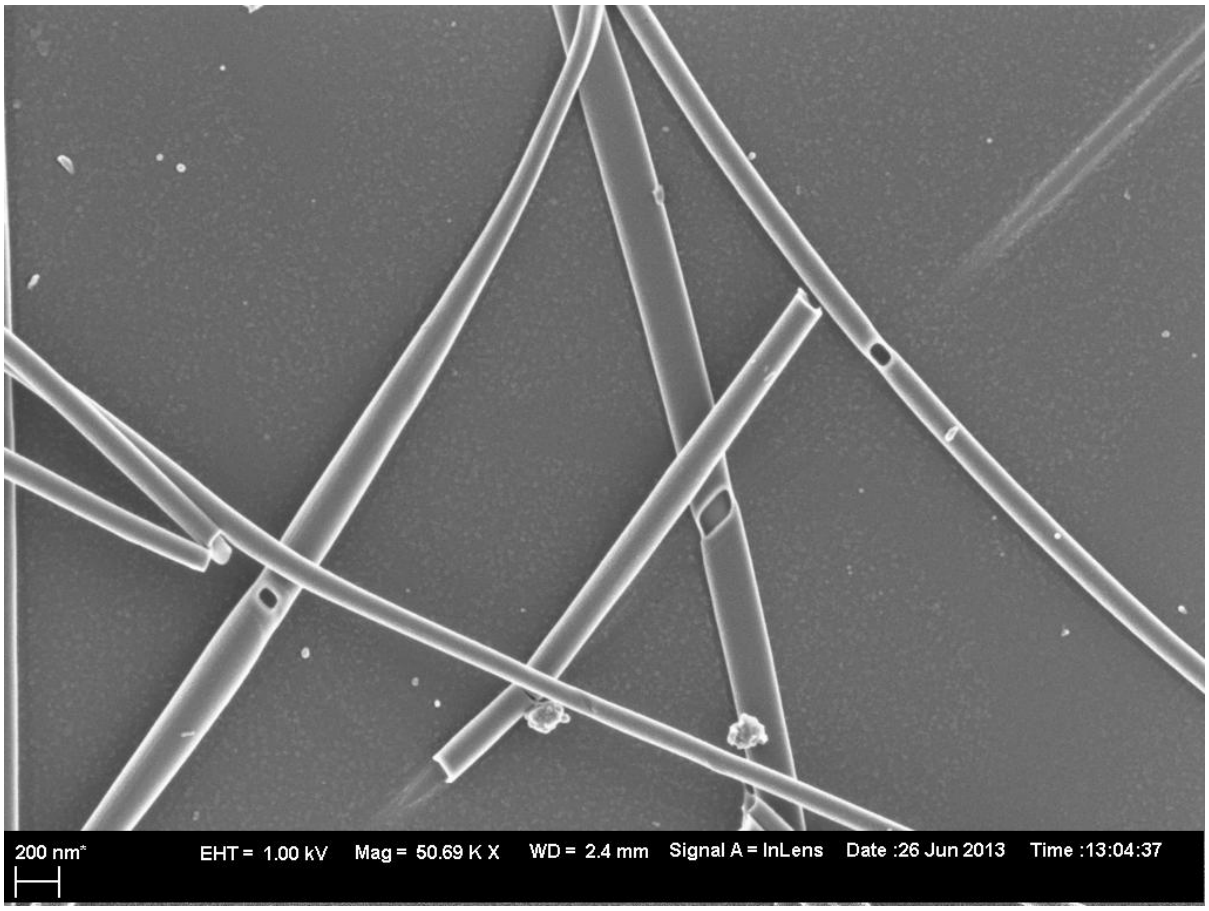

Figure 23. SEM image showing the hollow feature of the deposited fiber by electrospinning

In summary, the optimized conditions for best PVA fibers growth were: Concentration will be fixed at 10 wt%, flow rate will be 3 ml/h, applied voltage will be 30 kV, growth time of 60 s and tip/collector distance will be fixed at 12 cm. These parameters yielded hollow smooth fibers free of beads with diameter in the range of 190-340 nm.

4.2 ELECTROSPUN PVA/GRAPHENE NANO-FIBER

The optimized parameters for electrospinning of PVA fiber had also been used to grow PVA/graphene fibers. The objective here is to fill the tube with graphene in order to enhance

and/or modify the properties of the fibers. Figure 24 shows the schematic diagram for the fabrication of PVA/graphene composites by electrospinning. In section 3.5, we already explained the preparation process of the PVA/graphene solution using CVD derived graphene foam, expanded graphite and pure graphite powder and hence the graphene derived from these three different methods will be used as fillers in PVA fibers.

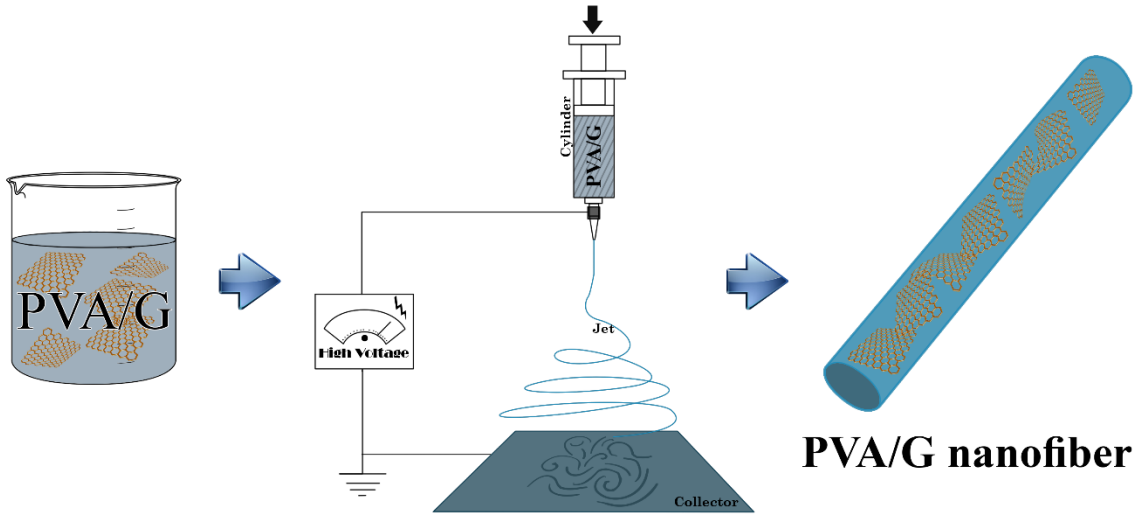

Figure 24. Schematic illustration of the fabrication of PVA/graphene nanofiber composite by electrospinning

4.2.1 Characterization of starting materials: Graphene foam, graphene derived from expanded graphite and pure graphite powder and PVA

Figure 25 shows the SEM micrographs of graphene foam (G1), graphite flakes derived from expanded graphite (G2) and pure graphite powder (G3) before dissolved in the PVA solution.

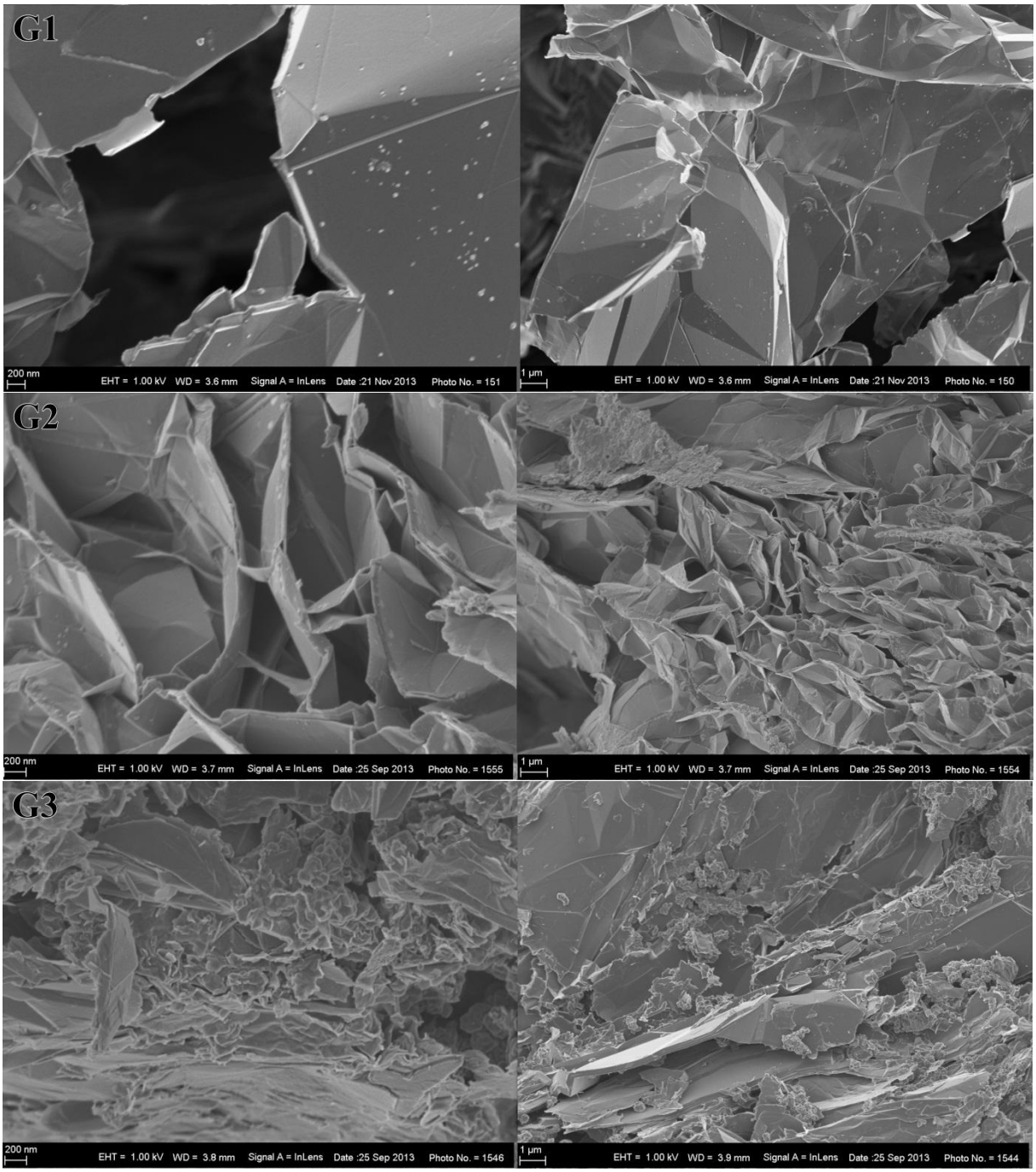

Figure 25. SEM micrographs of Graphene foam (G1), graphene derived from expanded graphite (G2) and pure graphite powder (G3) at different scales of 200 nm on the left and 1 µm on the right for each sample.

Raman spectroscopy is a versatile technique to characterize carbon materials. Figure 26 shows Raman spectra of raw materials, graphene foam, graphite flakes derived from derived from expanded graphite and pure graphite powder, respectively before being dissolved in PVA. All spectra show prominent peaks at around 1580 cm^{-1} (G-Peak) and 2700 cm^{-1} (2D-Peak). These peaks have been assigned to graphitic carbons with sp^2 hybridization [102,103]. In the case of disordered samples, the peak at around 1350 cm^{-1} (D-Peak) is observed. In this case, the graphene foam only shows two prominent peaks at 1580 cm^{-1} and 2700cm^{-1} but no D-Peak at 1350 cm^{-1}, which is a sign of defect high quality sample. For graphite flakes derived from expanded graphite and graphite powder, the peak at 1350 cm^{-1} is prominent indicating the presence of disorder in the samples which could be due to the presence of sp^3 or disorder due to the processing of the materials. The shape of 2D and also the intensity ratios between I_{2D} to I_G which is less than 1 for graphene foam show that the produced graphitic sample is couple of graphene layers instead of monolayer graphene.

Figure 27 shows the Raman spectrum of PVA. The peaks at around 1360 cm^{-1}, 1440 cm^{-1} correspond to the C-H and O-H bending while the peaks at around 2700 cm^{-1} and 2900 cm^{-1} are solely ascribed to the C-H stretching [104]. The 2700 cm^{-1} PVA Raman peak overlaps with 2D graphene peak which exists at the same wave number. Furthermore, the peaks at 1350 cm^{-1} in graphene and 1360 cm^{-1} in PVA are very close and are likely to overlap in the PVA/graphene spectrum. However, the scope of this work is not to thoroughly study the Raman but to confirm the presence of graphene fillers in the PVA nano-fibers.

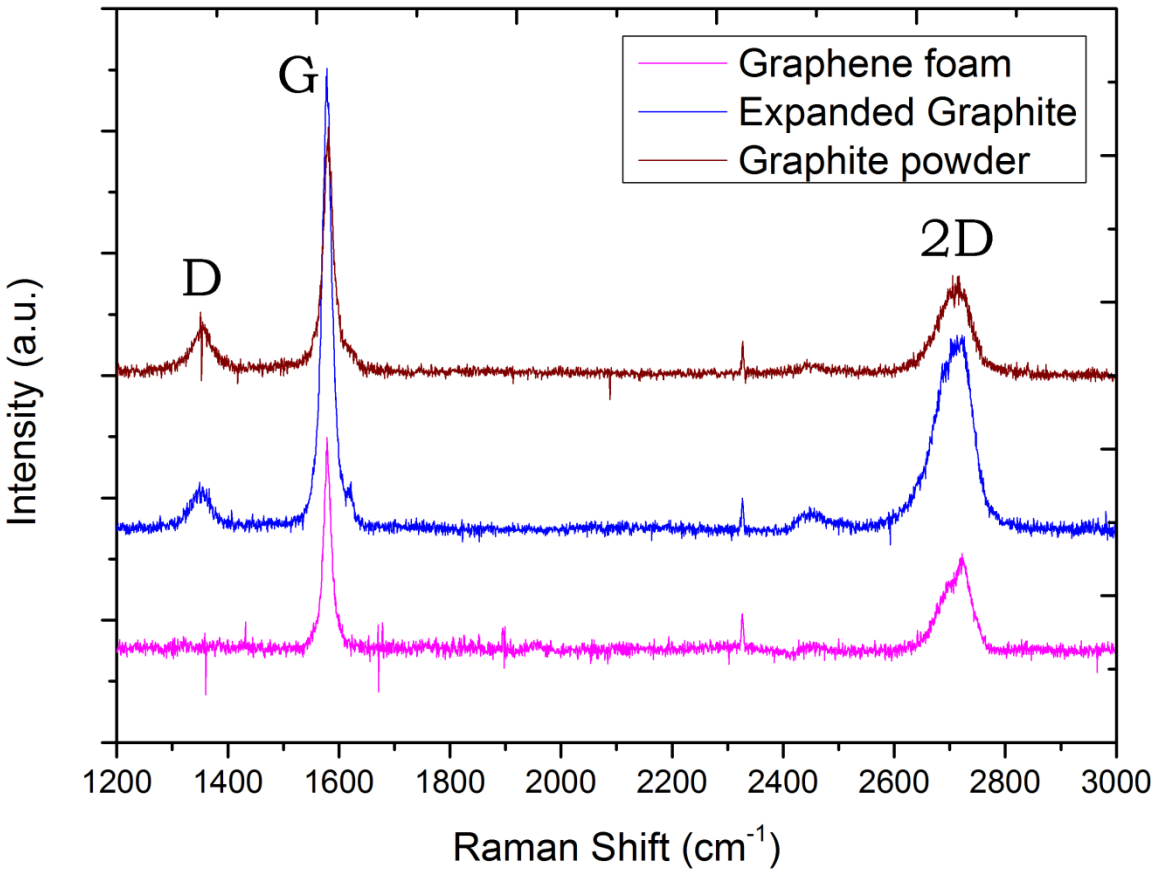

Figure 26. Raman spectra of graphene foam, graphene derived from expanded graphite and pure graphite powder

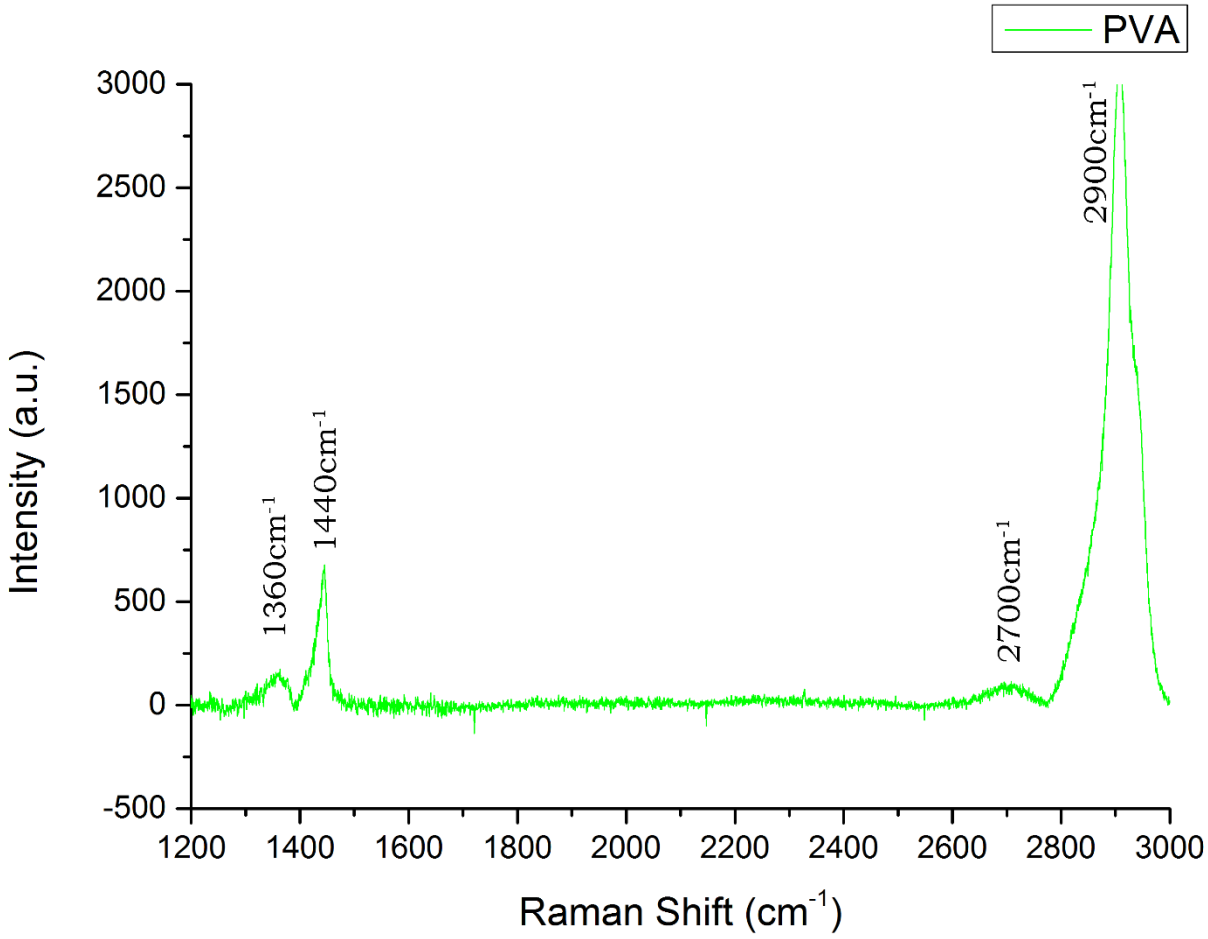

Figure 27. Raman spectrum of PVA

4.2.2 Synthesis and characterization of PVA/graphene composites solutions and their electrospun fibers

In section 3.5, the experimental procedure used to prepare the PVA/graphene foam, PVA/graphene derived from expanded graphite and graphite powder composites were explained. The optimized parameters that were decided to give best PVA parameters will be

fixed in the synthesis of PVA/grapene nano-fibers with only the concentration of the fillers being varied from 0.02 g to 0.08 g.

Figure 28 shows comparison of Raman spectra of PVA/graphene composites solution samples that were drop coated on glass substrate and dried for 15 minutes in oven at 60 ˚C. All prominent peaks from graphene and PVA as indicated in figures 25 and 26 above are still observed with exception of the reduction in intensity of G peak of graphene when dispersed dispersed in PVA solution. This reduction is a clear indication of interaction of graphene flakes with PVA molecules.

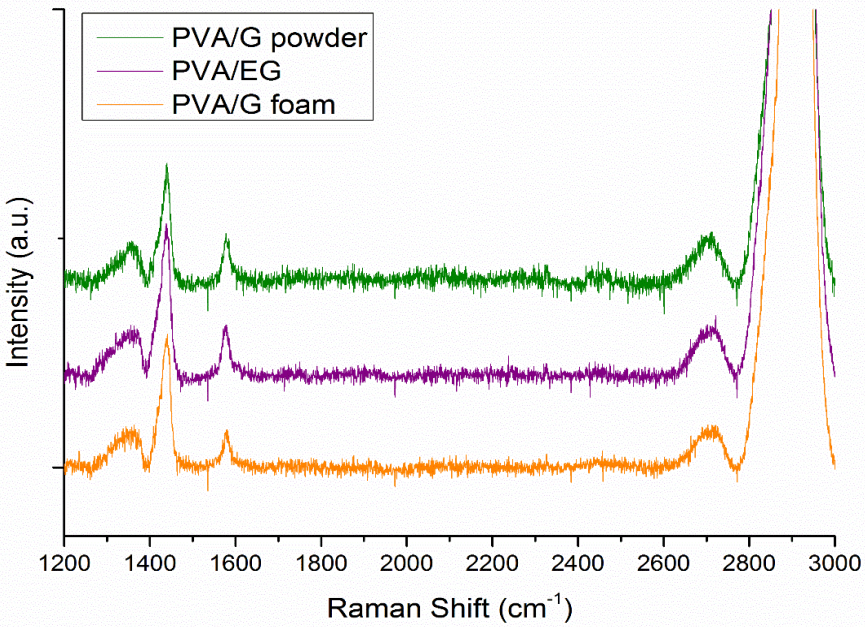

Figure 28 Raman spectra data comparison of PVA/graphene foam, PVA/graphene derived from expanded graphite and PVA/graphene derived from graphite powder

Figure 29 shows an example of the SEM morphology, taken at 1 kV operating voltage, of the fibers grown using 0.08 g graphene foam concentration with other concentrations giving similar continuous fibers without beads or droplets

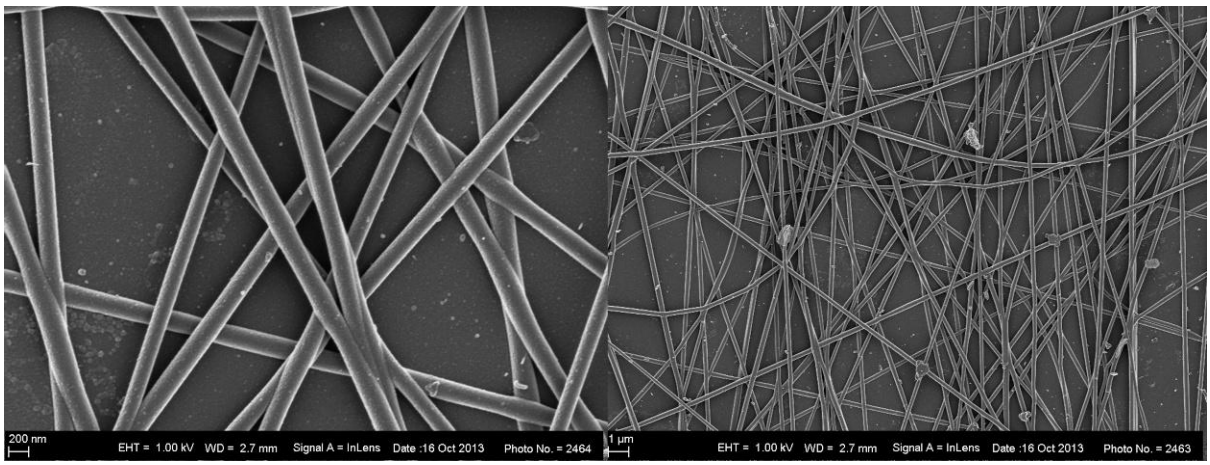

Figure 29. SEM micrograph example of one of the electrospun PVA/graphene foam fibers (from solution with 0.08 g graphene foam concentration)

In order to inspect if the graphene foam was indeed filled in the hollow PVA nano-fibers high magnification SEM of the fibers was taken. Figure 30 shows such SEM images at 2 kV for the two different concentrations of graphene foam in PVA solution. The figure shows two different contrast of the fibers with outer side of the fiber being lighter and inside consisting of dark dots as indicated by the arrows in the figures on each panel. It is also observed that these dark dots seem to connect to form continuous structure in the fiber as the graphene foam concentration is increased in the PVA solution (see Figure 30 b). This is the evidence that the observed dark dots aligned correspond to graphene foam flakes or particles being aligned in the PVA nano-fiber.

The diameters of the fibers were found to be in the range of 167 – 209 nm. These diameters are smaller than the diameters of the PVA fibers that were synthesized without incorporation of graphene in the solution. Since graphene is a material that has high conductivity, its incorporation into PVA solution enhances the conductivity of the solution to be electrospun and because of this improved conductivity the resulting fibers will normally be thinner.

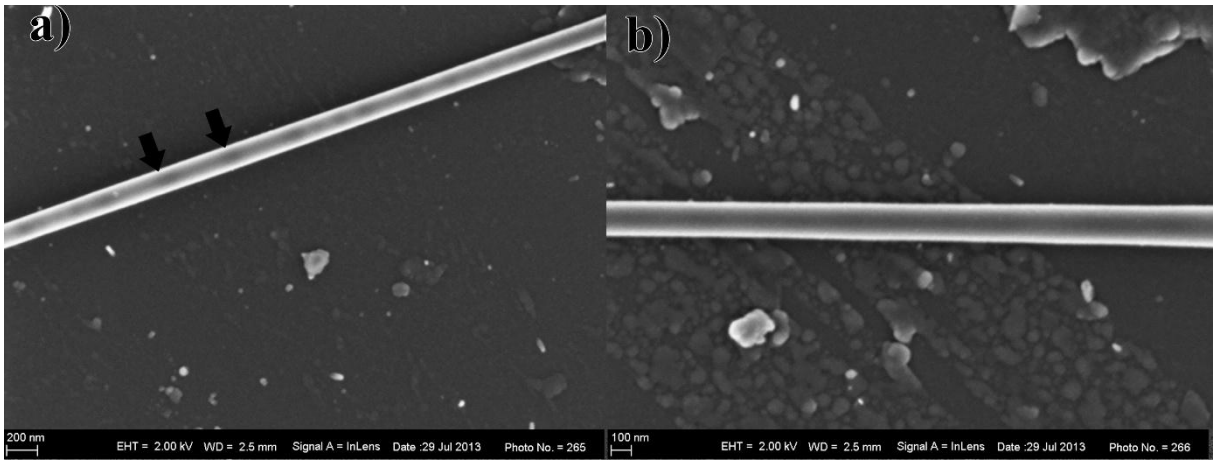

Figure 30. SEM micrographs of PVA/graphene foam nano-fibers at high operating voltage for (a) solution with 0.02 g graphene foam concentration (b) solution with 0.08 g graphene foam concentration

Figure 31 shows example of the fibers produced from 0.08 g expanded graphite concentration with fibers from other solution having similar morphology at 1 kV operating voltage. The diameter of the fibers here are in the range of 154 – 255 nm, which is also is smaller than the PVA fibers.

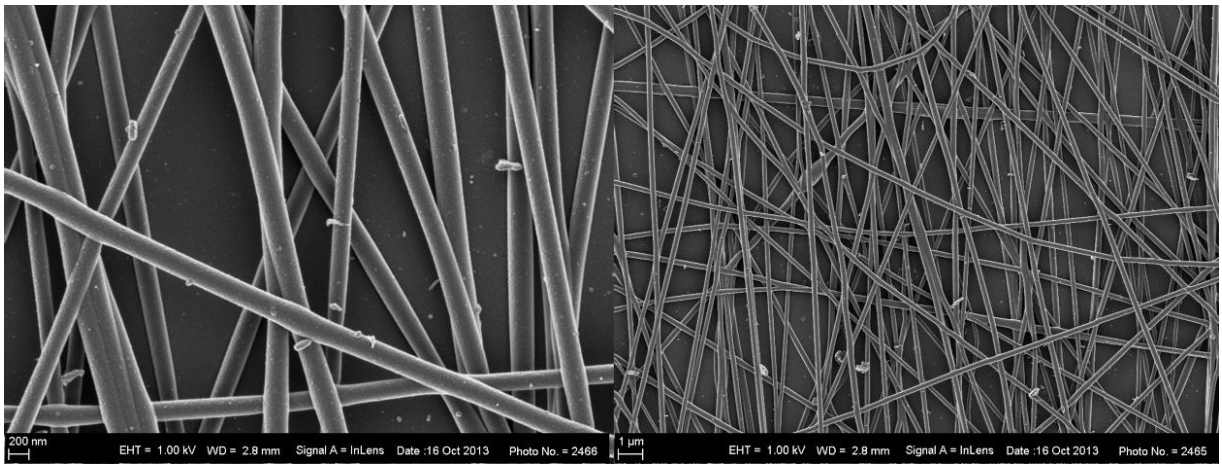

Figure 31. SEM micrograph example of one of electrospun PVA/graphene derived from expanded graphite fiber (from solution with 0.08 g expanded graphite concentration)

The graphene derived from expanded graphite concentration dependence in PVA solution for fibers production is shown in Figure 32 with 0.02 g and 0.08 g expanded graphite concentration in PVA solution respectively. Here also two different morphologies of the fibers are observed with outer part corresponding to PVA fiber walls being lighter and dark dots aligned inside the fibers. The concentration of aligned dark dots also increases with the increase of graphene derived from expanded graphite concentration. Again this can only mean that the dark dots in the fibers correspond to the graphene being incorporated in the PVA fibers.

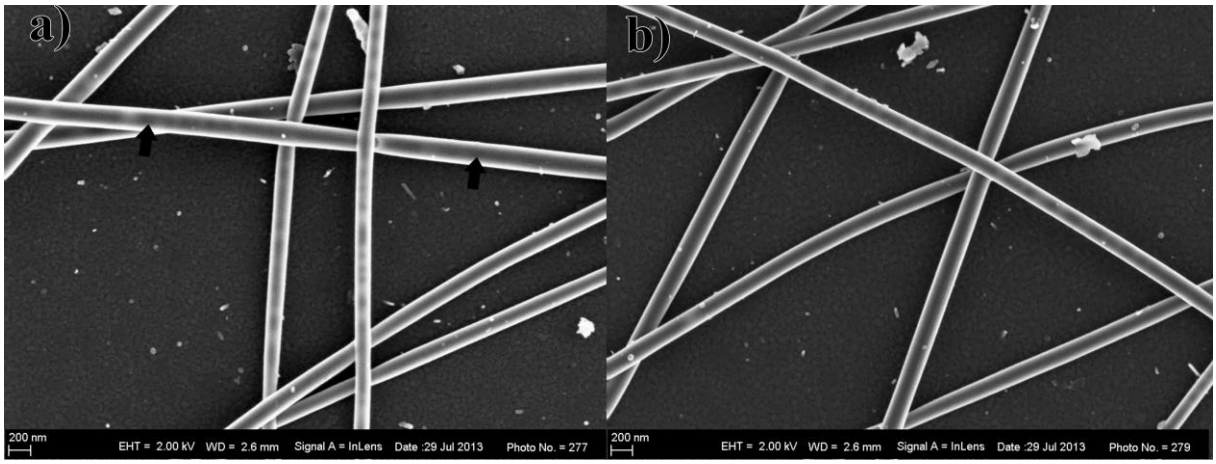

Figure 32. SEM micrographs of PVA/ graphene derive from expanded graphite at high operating voltage for (a) solution with 0.02 g expanded graphite concentration (b) solution with 0.08 g expanded graphite concentration

Figure 33 also shows an example of the fibers obtained by electrospinning PVA/graphene derived from graphite powder with 0.08 g graphite powder concentration with the rest of the fibers from other solution showing similar morphology at same operating voltage. The fibers from these materials had diameter in the range of 132 - 235 nm which are with the same range as the fibers from other composites discussed above.

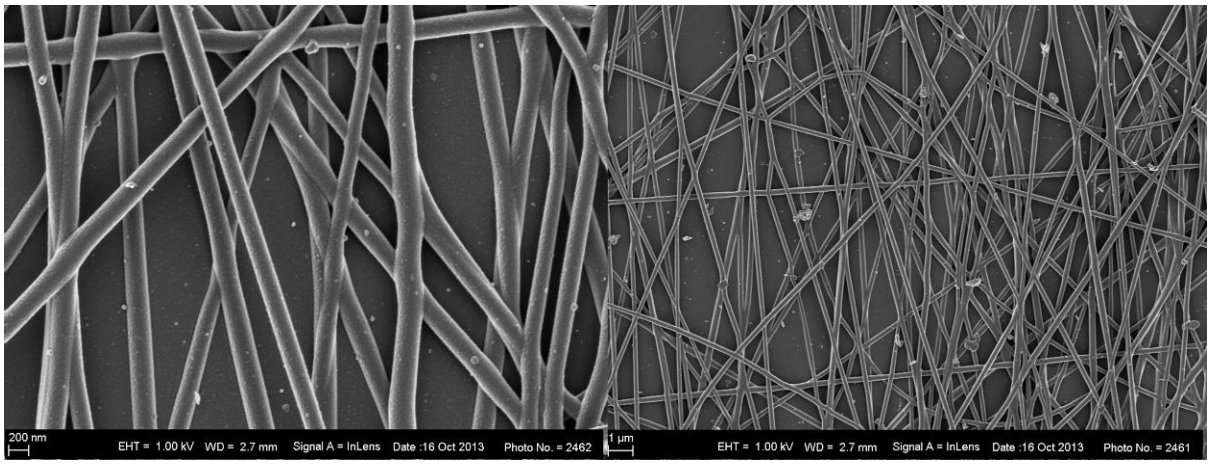

Figure 33. SEM micrograph example of electrospun PVA/graphene derived from graphite powder fiber (from solution with 0.08 g graphite powder concentration)

Figure 34 also shows the SEM micrograph at 2 kV operating voltage of the composite in this case for different graphene derived from graphite powder concentration. Like in the previous cases one can clearly see that graphene is inside the fibers forming dark spots which intensities and continuity increasing with the increasing concentration of graphene in the PVA solution.

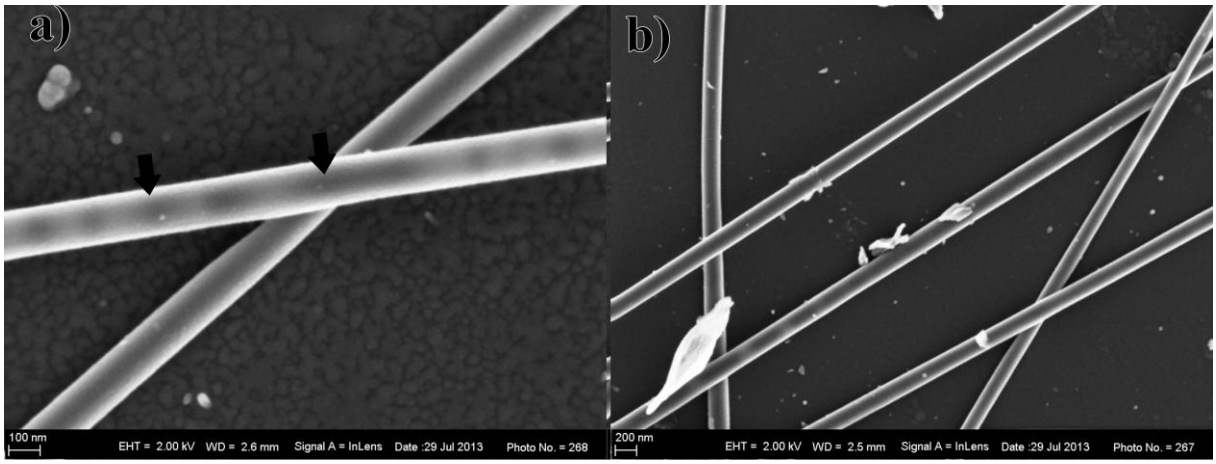

Figure 34. SEM micrographs of PVA/ graphene derive from graphite powder at high operating voltage for (a) solution with 0.02 g graphite powder concentration (b) solution with 0.08 g graphite powder concentration

4.2.3 Thermal Analysis of PVA/graphene composites comparison

4.2.3.1 Thermogravimetric Analysis comparison

Figures 34 and 35 shows typical TGA thermograms and corresponding first order derivative (DTGA) of weight loss as a function of temperature for PVA with and without graphene fillers respectively. The samples were measured in the temperature range from 25 $^{\circ}$C up to 1000 $^{\circ}$C with a constant rate of 10 $^{\circ}$C/min in air. TGA and DTGA show that all samples exhibit three distinct weight loss stages as dictated in the Table 16 for different PVA/graphene composites: ~25 – 145 $^{\circ}$C corresponds to loss of moisture, physisorbed, and chemisorbed water molecules [105], ~145 – 391 $^{\circ}$C corresponds to decomposition of the side chains of PVA (in this stage two peaks are observed with first peak corresponding to the loss of H bond

between PVA molecules and second peak to the loss of O bond between C-O) and ~391 – 573 °C corresponding to the decomposition of the main chain of PVA [106,107].

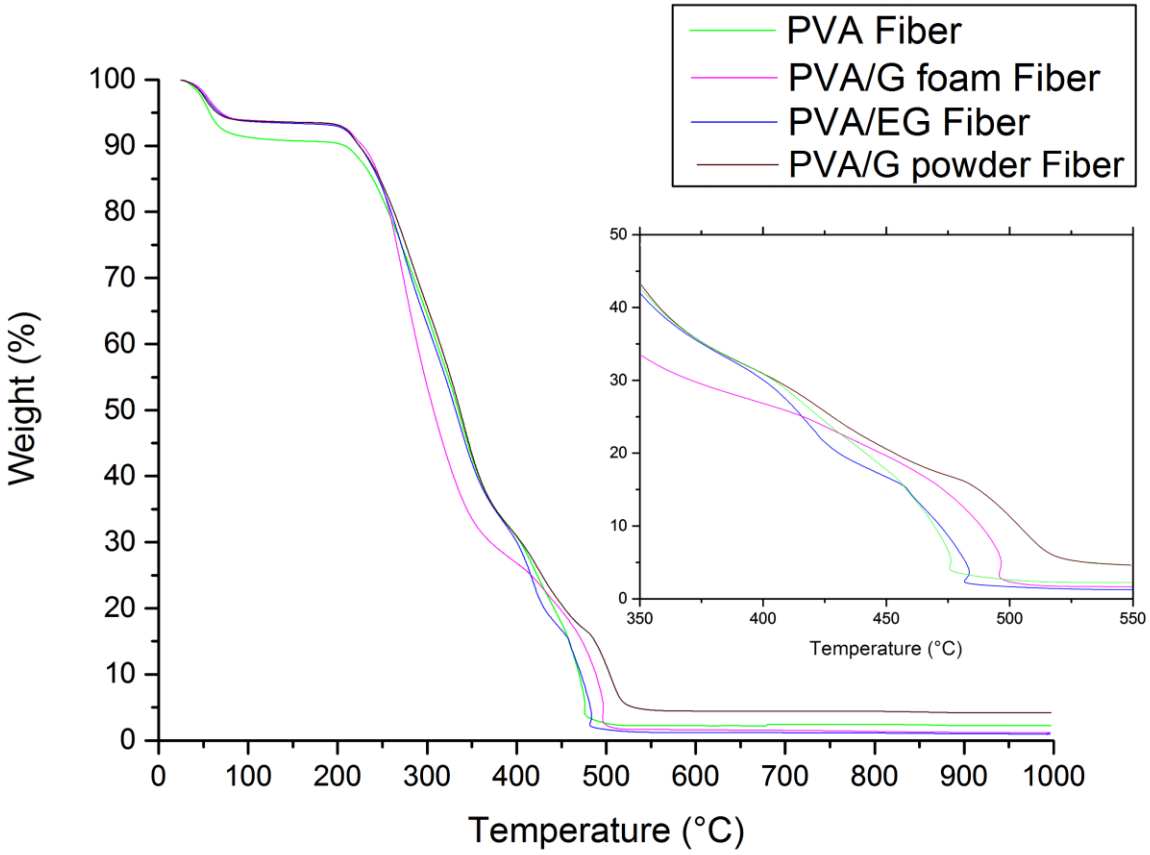

Figure 35. TGA curves for electrospun PVA fibers with and without graphene fillers.

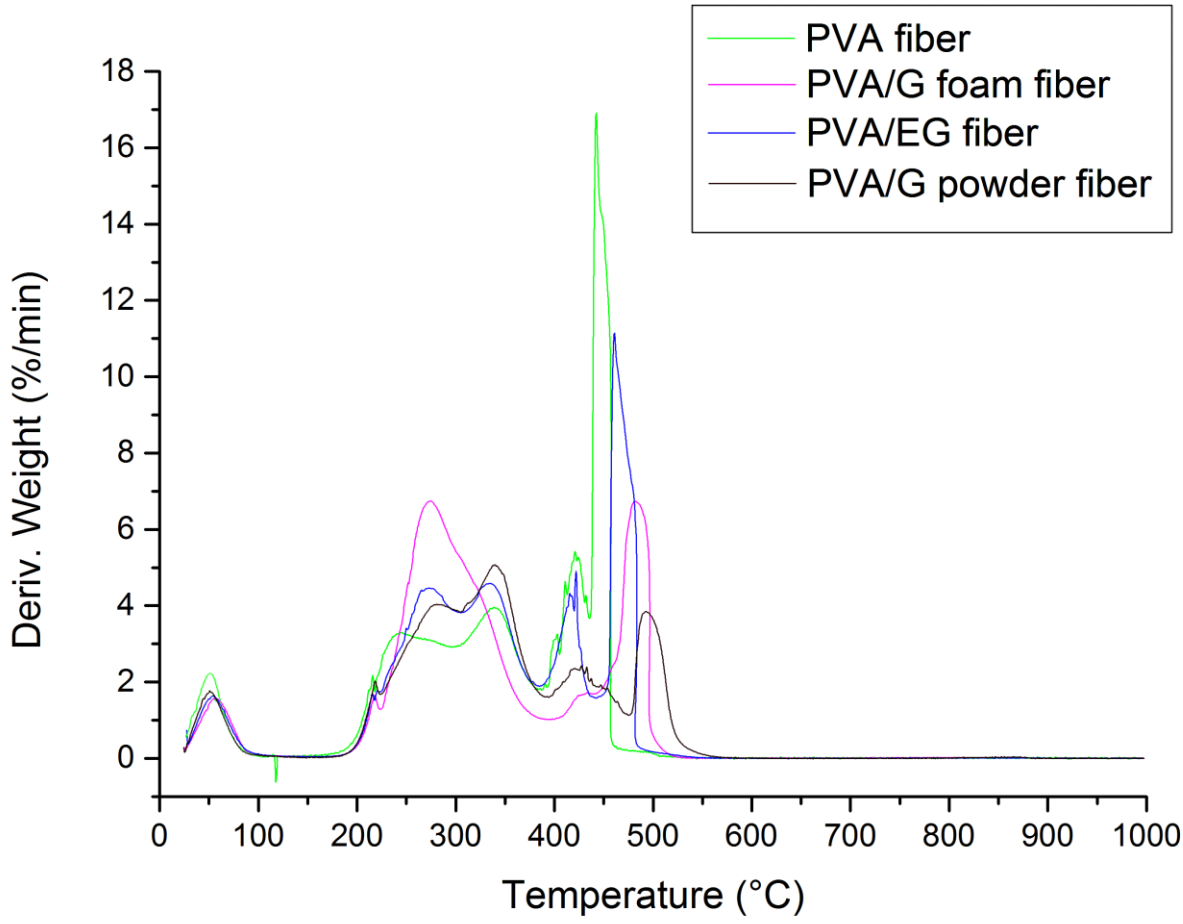

Figure 36 The first order derivative of TGA for electrospun PVA fibers with and without graphene fillers.

Figure 36 shows the first order derivatives of TGA curves. The trend for weight loss was the same for all samples. The sheet structure of graphene may act as diffusion barrier suppressing the decomposition of PVA, resulting in increased decomposition temperature. On the other hand, the samples are nanofibers with diameters of only around 130–250 nm and the 2D sp^2 sheet structure of graphene helps the chain of PVA to stay intact at higher temperatures. At 600 $^{\circ}$C and above, all TGA diagrams become flat and mainly carbon residue remains.

Table 16 Degradation temperature of the baseline PVA and different graphene-loaded PVA fiber

Samples	**First stage lose weight (˚C)**	**Second stage lose weight (˚C)**	**Third stage lose weight (˚C)**
PVA fiber	25 - 124	124 - 383	383 – 460
PVA/G foam fiber	25 - 143	143 - 393	393 – 542
PVA/EG fiber	25 – 141	141 - 384	384 – 559
PVA/G powder fiber	25 - 145	145 - 391	391 – 573

Evidently, the thermal decomposition of electrospun PVA/graphene composites fibers shift to the higher temperature range compared to electrospun PVA fibers. This implies that the incorporation of graphene in PVA for electrospun fibers enhanced the thermal stability of electrospun PVA nanofibers. This thermal reinforcement of electrospun PVA fibers by nano-carbon fillers is very important for polymer nanofibers in different technological applications such as those mentioned in the introduction section.

CHAPTER 5

Summary and conclusions

In this thesis, we successfully incorporated graphene nanofillers into PVA fibers in order to improve the thermal properties of the resulting fibers. Three different source of graphene were used for that purpose and all show improved thermal properties of the fibers after incorporation of graphene nanofillers.

The relatively simple and economical electrospinning technique was used to fabricate continuous fibers. The growth of the PVA fibers was optimized for this system in terms of bead free fibers and thinner fibers. These optimum parameters which are 10 wt% for PVA concentration, 3 ml/h for the solution flow rate, 30 kV for applied voltage, growth time of 60 s and 12 cm for tip/collector distance, were then used to grow PVA/graphene fibers. In other words, it was observed that higher polymer concentration solution, for example 12 wt% PVA, produces thicker electrospun fibers. Lower flow rates produce thinner electrospun fibers but with beads. The strong electric field makes the liquid jet thinner, resulting in decreasing of the average diameter of fibers and therefore produces thinner fibers. If non-conductive polymer like PVA is used, longer growth time increases the diameter of the fibers. For shorter needle tip/collector distance, the fiber does not have enough time to dry and consequently the diameter of the fibers increase whereas when this distance is increased, it gives more time for the fibers to dry during spinning. However, further increase in this distance results in lower electric field effect which thickens the fibers. Furthermore, the addition of graphene to the

solution produces thinner electrospun fibers. The phenomenon is related to the enhanced conductivity of the electrospun solution.

The incorporation of the graphene nanofillers was possible because of the hollow structure from the PVA fiber as observed under SEM. Furthermore, electrospun PVA/graphene fibers show dark space inside the fibers which is related to the graphene nanofillers. Continuous nanofillers are observed for higher graphene concentration in the electrospun PVA/graphene solution.

The presence of graphene nanofillers was further confirmed by TGA. Enhanced thermal properties was observed when PVA/graphene solutions was used for producing the fibers. TGA results show a slow weight loses, meaning enhanced thermal stability of the fibers with increasing graphene loading into the PVA fibers.

Future work

The fibers produced by this method are promising for use in electrodes, conductive wires, smart fabrics, and other applications which require conductive filler inside the polymer nanofibers [16]. For future work, conductive polymer such as polypyrrole (PPY) will be used for better control of the diameter of the fibers produced. The effect of graphene nanofillers on the PPY conductive fibers will be investigated.

These conductive PPY/graphene fibers are also good candidate for electrode material for energy storage device such as supercapacitors, since they present a high surface area, high conductivity and porosity. Therefore, the fibers produced will be tested for this application.

Reference

[1] Mark H F 1986 Encyclopedia of polymer science and engineering, book, 192-233

[2] Bacon R and Moses C T 1986 High Performance Polymers: Their Origin and Development, book, 341-353

[3] Ramakrishna S 2005 An introduction to electrospinning and nanofibers, book

[4] Novoselov K S, Geim a K, Morozov S V, Jiang D, Zhang Y, Dubonos S V, Grigorieva I V and Firsov a a 2004 Electric field effect in atomically thin carbon films Science 306 666–669

[5] Geim a K and Novoselov K S 2007 The rise of graphene Nat. Mater. 6 183–191

[6] Baughman R H, Zakhidov A a and de Heer W a 2002 Carbon nanotubes--the route toward applications. Science 297 787–792

[7] Kaneto K, Tsuruta M, Sakai G, Cho W and Ando Y 1999 Electrical conductivities of multi-wall carbon nano tubes Synth. Met. 103 2543–2546

[8] Bajáková J, Chaloupek J, Lukáš D and Lacarin M 2011 „Drawing "-the production of individual nanofibers by experimental method nanocon.eu

[9] Formhals A 1934 Process and apparatus for preparing artificial threads: US Pat, 1975504

[10] Formhals A 1939 Method and apparatus for spinning US Pat. 2,160,962

[11] Foemhals A 1940 Artificial thread and method of producing same: US Pat, 2187306

[12] Formhals A 1943 Production of artificial fibers from fiber forming liquids: US Pat, 2323025

[13] Formhals A 1944 Method and apparatus for spinning US Pat. 2,349950

[14] Fong H, Chun I and Reneker D . 1999 Beaded nanofibers formed during electrospinning Polymer (Guildf). 40 4585–4592

[15] Das S, Wajid A S, Bhattacharia S K, Wilting M D, Rivero I V. and Green M J 2013 Electrospinning of polymer nanofibers loaded with noncovalently functionalized graphene J. Appl. Polym. Sci. 128 4040–4046

[16] Chowdhury M and Stylios G 2010 Effect of experimental parameters on the morphology of electrospun Nylon 6 fibres Int. J. Basic Appl. … 70–78

[17] Wang C, Li Y, Ding G, Xie X and Jiang M 2013 Preparation and characterization of graphene oxide/poly(vinyl alcohol) composite nanofibers via electrospinning J. Appl. Polym. Sci. 127 3026–3032

[18] Sui X-M, Giordani S, Prato M and Wagner H D 2009 Effect of carbon nanotube surface modification on dispersion and structural properties of electrospun fibers Appl. Phys. Lett. 95 233113

[19] Costa S 2008 Characterization of carbon nanotubes by Raman spectroscopy Mater Sci …26 433-441

[20] Ebbesen T W 1996 Carbon Nanotubes Phys. Today 26–32

[21] Sahoo S, Dhibar S, Hatui G, Bhattacharya P and Das C K 2013 Graphene/polypyrrole nanofiber nanocomposite as electrode material for electrochemical supercapacitor Polymer (Guildf). 54 1033–1042

[22] Katsnelson M 2007 Graphene: carbon in two dimensions Mater. today 10 20–7

[23] Huh D S, Basavaraja C and Jung K W Polypyrrole / graphene oxide composites with improved conductivity and solubility 50 10–1

[24] Xu Y, Hong W, Bai H, Li C and Shi G 2009 Strong and ductile poly(vinyl alcohol)/graphene oxide composite films with a layered structure Carbon N. Y. 47 3538–3543

[25] Soldano C, Mahmood A and Dujardin E 2010 Production, properties and potential of graphene Carbon N. Y. 48 2127–2150

[26] Ramanathan T, Abdala a a, Stankovich S, Dikin D a, Herrera-Alonso M, Piner R D, Adamson D H, Schniepp H C, Chen X, Ruoff R S, Nguyen S T, Aksay I a, Prud'Homme R K and Brinson L C 2008 Functionalized graphene sheets for polymer nanocomposites Nat. Nanotechnol. 3 327–331

[27] Peijs T, Vught R Van and Govaert L 1995 Mechanical properties of poly (vinyl alcohol) fibres and composites Composites 26 83–90

[28] Wang J, Wang X, Xu C, Zhang M and Shang X 2011 Preparation of graphene/poly(vinyl alcohol) nanocomposites with enhanced mechanical properties and water resistance Polym. Int. 60 816–822

[29] Anish Madhavan A, Kalluri S, K Chacko D, Arun T a., Nagarajan S, Subramanian K R V., Sreekumaran Nair a., Nair S V. and Balakrishnan A 2012 Electrical and optical properties of electrospun TiO2-graphene composite nanofibers and its application as DSSC photo-anodes RSC Adv. 2 13032

[30] Salles V, Seveyrat L, Fiorido T, Hu L and Galineau J 2012 Synthesis and characterization of advanced carbon-based nanowires–study of composites actuation capabilities containing these nanowires as fillers nanowires - Recent Adv. 295-303

[31] Fuchs J and Goerbig M 2008 Introduction to the physical properties of graphene Lect. Notes

[32] Vollhardt K and Schore N 2007 Organic chemistry: structure and function, book

[33] Viculis L M, Mack J J, Mayer O M, Hahn H T and Kaner R B 2005 Intercalation and exfoliation routes to graphite nanoplatelets J. Mater. Chem. 15 974-978

[34] Huang L, Wu B, Yu G and Liu Y 2011 Graphene: learning from carbon nanotubes J. Mater. Chem. 21 919-929

[35] Yasmin A, Luo J-J and Daniel I M 2006 Processing of expanded graphite reinforced polymer nanocomposites Compos. Sci. Technol. 66 1179–1186

[36] Duplock E, Scheffler M and Lindan P 2004 Hallmark of perfect graphene Phys. Rev. Lett. 92 225502

[37] Novoselov K, Geim A and Morozov S 2005 Two-dimensional gas of massless Dirac fermions in graphene Nature 438, 197-200

[38] Liang J, Huang Y, Zhang L, Wang Y, Ma Y, Guo T and Chen Y 2009 Molecular-Level Dispersion of graphene into Poly(vinyl alcohol) and effective reinforcement of their nanocomposites Adv. Funct. Mater. 19 2297–2302

[39] Wakabayashi K, Brunner P J, Masuda J, Hewlett S a. and Torkelson J M 2010 Polypropylene-graphite nanocomposites made by solid-state shear pulverization: Effects of significantly exfoliated, unmodified graphite content on physical, mechanical and electrical properties Polymer (Guildf). 51 5525–31

[40] Utracki L A 2003 Polymer blends handbook ed L A Utracki (Dordrecht: Springer Netherlands) , book

[41] Billmeyer F 1984 Textbook of polymer science, book

[42] Cowie J 1991 Polymers: chemistry and physics of modern materials, book

[43] Wool R and Sun X 2011 Bio-based polymers and composites, book

[44] Brinchi L, Cotana F, Fortunati E and Kenny J M 2013 Production of nanocrystalline cellulose from lignocellulosic biomass: technology and applications. Carbohydr. Polym. 94 154–69

[45] Baillie C 2004 Green composites Polymer composites and the environment, book

[46] MacGregor E and Greenwood C 1980 Polymers in nature, book

[47] Sperling L 2005 Introduction to physical polymer science, book

[48] Shaw M and MacKnight W 2005 Introduction to polymer viscoelasticity, book

[49] Bower D I 2002 An Introduction to Polymer Physics (Cambridge: Cambridge University Press) , book

[50] Flory and J. P 1953 Principles of polymer chemistry, book

[51] Feller R, Stolow N and Jones E 1971 On picture varnishes and their solvents

[52] Xie Y, Qiao Z, Chen M, Zhu Y and Qian Y T 2000 Spherical assemblies of CdS nanofibers in poly (vinyl acetate) by ɤ-irradiation 11 1165–1169

[53] Abu-Saied M, Khalil K and Al-Deyab S 2012 Preparation and characterization of Poly Vinyl Acetate nanofiber doping copper metal Int. J. Electrochem. Sci 7 2019–2027

[54] Lindemann M 1989 Vinyl acetate and the textile industry Text. Chem. Colour 21-28

[55] Wang G, Tan Z, Liu X, Chawda S, Koo J-S, Samuilov V and Dudley M 2006 Conducting MWNT/poly(vinyl acetate) composite nanofibres by electrospinning Nanotechnology 17 5829–5835

[56] Peijs T 1995 Mechanical properties of poly(vinyl alcohol) fiber and composite Composites 26 83–90

[57] Misra G and Mukherjee P 1980 The relation between the molecular weight and intrinsic viscosity of polyvinyl alcohol Colloid Polym. Sci. 155 152–155

[58] Efimov O, Search H, Journals C, Contact A, Iopscience M and Address I P 1997 Polypyrrole: a conducting polymer; its synthesis, properties and applications Russ. Chem. Rev. 443

[59] Singh R N and Awasthi R 2011 Polypyrrole Composites : Electrochemical synthesis , characterizations and applications electropolymerization pp 131–158

[60] Eisazadeh H, Engineering C and Box P O 2007 Studying the characteristics of Polypyrrole and its composites World J. Chem. 2 67–74

[61] Street G B, Clarke T C, Geiss R H, Lee V Y, Nazzal a., Pfluger P and Scott J C 1983 Characterization of Polypyrrole Le J. Phys. Colloq. 44 599–606

[62] Yu E H and Sundmacher K 2007 Enzyme electrodes for glucose oxidation prepared by electropolymerization of Pyrrole Process Saf. Environ. Prot. 85 489–493

[63] MacDiarmid A 2001 “Synthetic metals”: A novel role for organic polymers (Nobel lecture) Angew. Chemie Int. Ed.

[64] Jorio A, Dresselhaus G and Dresselhaus M 2008 Carbon nanotubes: advanced topics in the synthesis, structure, properties and applications, book

[65] Koziol K, Boskovic B and Yahya N 2011 Synthesis of carbon nanostructures by CVD method Carbon and Oxide Nanostructures 414-428

[66] Che G, Lakshmi B B, Martin C R, Fisher E R and Ruoff R S 1998 Chemical vapor deposition based synthesis of carbon nanotubes and nanofibers using a template method 4756 260–267

[67] Guermoune A, Chari T, Popescu F, Sabri S S, Guillemette J, Skulason H S, Szkopek T and Siaj M 2011 Chemical vapor deposition synthesis of graphene on copper with methanol, ethanol, and propanol precursors Carbon N. Y. 49 4204–4210

[68] Zhang Y, Zhang L and Zhou C 2013 Review of chemical vapor deposition of graphene and related applications Acc. Chem. Res.2329-2339

[69] Ondarcuhu T, Joachim C and Cnrs C 1998 Drawing a single nanofibre over hundreds of microns EPL (Europhysics Lett. 215 215–220

[70] Huang Z-M, Zhang Y-Z, Kotaki M and Ramakrishna S 2003 A review on polymer nanofibers by electrospinning and their applications in nanocomposites Compos. Sci. Technol. 63 2223–2253

[71] Anon research.chem.psu.eduaxsgroupRanresearchtemplatesynthesis.html-2014

[72] Hartgerink J D, Beniash E and Stupp S I 2001 Self-assembly and mineralization of peptide-amphiphile nanofibers Science 294 1684–1688

[73] Sundaray B, Ph D, Babu V J, Subramanian V and Natarajan T S 2008 Preparation and characterization of electrospun fibers of Poly (methyl methacrylate) - single walled carbon nanotube nanocomposites 39-45

[74] Pham Q P, Sharma U and Mikos A G 2006 Electrospinning of polymeric nanofibers for tissue engineering applications: a review. Tissue Eng. 12 1197–1211

[75] Reneker D H and Chun I 1996 Nanometre diameter fibres of polymer, produced by electrospinning Nanotechnology 7 216–223

[76] Michelson D, Robbins M S and Bradley R M 1993 On the stability of the Taylor cone J. Aerosol Sci. 24 491–492

[77] Gañán-Calvo a M, Rebollo-Muñoz N and Montanero J M 2013 The minimum or natural rate of flow and droplet size ejected by Taylor cone–jets: physical symmetries and scaling laws New J. Phys. 15 1-11

[78] Cloupeau M and Prunet-Foch B 1994 Electrohydrodynamic spraying functioning modes: a critical review J. Aerosol Sci. 25 1021–1036

[79] Jayasinghe S N and Edirisinghe M J 2004 Electrostatic atomisation of a ceramic suspension J. Eur. Ceram. Soc. 24 2203–2213

[80] Gañán-Calvo A 1997 Cone-Jet analytical extension of taylor's electrostatic solution and the asymptotic universal scaling laws in electrospraying Phys. Rev. Lett. 79 217–220

[81] Nayyar N K and Murty G S 1960 The stability of a dielectric liquid jet in the presence of a longitudinal electric field Proc. Phys. Soc. 369 369–373

[82] Perez a. T, Vazquez P a. and Castellanos a. 1995 Dynamics and linear stability of charged jets in dielectric liquids IEEE Trans. Ind. Appl. 31 761–767

[83] Shiryaeva S O 2010 On the capillary stability of a cylindrical dielectric liquid jet in a longitudinal electrostatic field Tech. Phys. 55 204–209

[84] Hohman M M, Shin M, Rutledge G and Brenner M P 2001 Electrospinning and electrically forced jets. I. Stability theory Phys. Fluids 13 2201-2220

[85] Hohman M M, Shin M, Rutledge G and Brenner M P 2001 Electrospinning and electrically forced jets. II. Applications Phys. Fluids 13 2221-2236

[86] Shin Y M, Hohman M M, Brenner M P and Rutledge G C 2001 Experimental characterization of electrospinning: the electrically forced jet and instabilities Polymer (Guildf). 42 9955–9967

[87] Li D, Wang Y and Xia Y 2003 Electrospinning of polymeric and ceramic nanofibers as uniaxially aligned arrays Nano Lett. 3 1167–1171

[88] Neo Y P, Ray S, Easteal A J, Nikolaidis M G and Quek S Y 2012 Influence of solution and processing parameters towards the fabrication of electrospun zein fibers with sub-micron diameter J. Food Eng. 109 645–651

[89] Tan S-H, Inai R, Kotaki M and Ramakrishna S 2005 Systematic parameter study for ultra-fine fiber fabrication via electrospinning process Polymer (Guildf). 46 6128–6134

[90] Thoppey N and Gorga R 2012 Effect of solution parameters on spontaneous jet formation and throughput in edge electrospinning from a fluid-filled bowl Macromolecules 45 6527–6537

[91] Megelski S, Stephens J S, Chase D B and Rabolt J F 2002 Micro- and nanostructured surface morphology on electrospun polymer fibers Macromolecules 35 8456–8466

[92] Zargham S, Bazgir S and Tavakoli A 2012 The effect of flow rate on morphology and deposition area of electrospun nylon 6 nanofiber Eng. Fibers Fabr. 7 42–49

[93] Karakaş H, Saraç A, Polat T and Budak E 2013 Polyurethane nanofibers obtained by electrospinning process waset.org 75 607–610

[94] Henriques C and Vidinha R 2009 A systematic study of solution and processing parameters on nanofiber morphology using a new electrospinning apparatus Nanosci. Nanotechnol. 8 1–11

[95] Basu S 2012 Understanding the effect of electrospinning distance on the morphology of the PAN nanofibers Spring, Conference 2012: Fiber Research for Tomorrow's Applications

[96] Dao A and Jirsak O 2010 Roller electrospinning in various ambient parameters Nanocon2010 Conf. 10–15

[97] Zhou W, Apkarian R P and Wang Z L Fundamentals of Scanning Electron Microscopy, book

[98] Coats A W and Redfern J P 1963 Thermogravimetric analysis analyst 88 906–924

[99] Bello a., Makgopa K, Fabiane M, Dodoo-Ahrin D, Ozoemena K I and Manyala N 2013 Chemical adsorption of NiO nanostructures on nickel foam-graphene for supercapacitor applications J. Mater. Sci. 48 6707–6712

[100] McCann J T, Li D and Xia Y 2005 Electrospinning of nanofibers with core-sheath, hollow, or porous structures J. Mater. Chem. 15 735-738

[101] Srivastava Y, Loscertales I, Marquez M and Thorsen T 2007 Electrospinning of hollow and core/sheath nanofibers using a microfluidic manifold Microfluid. Nanofluidics 4 245–520

[102] Ferrari A C 2007 Raman spectroscopy of graphene and graphite: Disorder, electron–phonon coupling, doping and nonadiabatic effects Solid State Commun. 143 47–57

[103] Malard L M, Pimenta M a., Dresselhaus G and Dresselhaus M S 2009 Raman spectroscopy in graphene Phys. Rep. 473 51–87

[104] Thomas P and Stuart B 1997 A Fourier transform Raman spectroscopy study of water sorption by poly (vinyl alcohol) … Part A Mol. Biomol. Spectrosc 2275-2278

[105] Anbarasan R 2010 Synthesis, characterizations, and mechanical properties of structurally modified poly (vinyl alcohol) . Appl. Polym. 2059–2068

[106] Sui X M, Shao C L and Liu Y C 2005 White-light emission of polyvinyl alcohol/ZnO hybrid nanofibers prepared by electrospinning Appl. Phys. Lett. 87 113-115

[107] Kumar A 2010 Fabrication of Bio-nanocomposite nanofibers mimicking the mineralized hard tissues via electrospinning process , Nanofiber book, 79-83